HHS Public Access

Author manuscript

Pain. Author manuscript; available in PMC 2022 April 11.

Published in final edited form as:

Pain. 2019 July ; 160(7): 1644–1661. doi:10.1097/j.pain.0000000000001524.

Targeting the CaVα–CaVβ interaction yields an antagonist of the N-type CaV2.2 channel with broad antinociceptive efficacy

Rajesh Khanna[a,b,c,d,*], **Jie Yu**[a,e], **Xiaofang Yang**[a], **Aubin Moutal**[a], **Aude Chefdeville**[a], **Vijay Gokhale**[b], **Zunaira Shuja**[e], **Lindsey A. Chew**[a], **Shreya S. Bellampalli**[a], **Shizhen Luo**[a], **Liberty François-Moutal**[a], **Maria J. Serafini**[a], **Taehwan Ha**[f], **Samantha Perez-Miller**[a], **Ki Duk Park**[f,g,h], **Amol M. Patwardhan**[a,c], **John M. Streicher**[a], **Henry M. Colecraft**[i,j], **May Khanna**[a,d]

[a]Department of Pharmacology, College of Medicine, University of Arizona, Tucson, AZ, United States,

[b]The BIO5 Institute, University of Arizona, Tucson, AZ, United States,

[c]Department of Anesthesiology, College of Medicine, University of Arizona, Tucson, AZ, United States,

[d]The Center for Innovation in Brain Sciences, The University of Arizona Health Sciences, Tucson, AZ, United States,

[e]College of Basic Medical Science, Zhejiang Chinese Medical University, Hangzhou, China,

[f]Convergence Research Center for Dementia, Korea Institute of Science and Technology, Seoul, Korea,

[g]Division of Bio-Medical Science and Technology, KIST School, Korea University of Science and Technology, Seoul, Korea,

[h]KHU-KIST Department of Converging Science and Technology, Kyung Hee University, Seoul, Korea,

[i]Department of Physiology and Cellular Biophysics, Columbia University College of Physicians and Surgeons, New York, NY, United States

[j]Pharmacology, Columbia University College of Physicians and Surgeons, New York, NY, United States

Abstract

[*]Corresponding author. Address: Department of Pharmacology, College of Medicine, University of Arizona, 1501 North Campbell Dr, P.O. Box 245050, Tucson, AZ 85724, United States. Tel.: (520) 626-4281; fax: (520) 626-2204. rkhanna@email.arizona.edu (R. Khanna).

Supplemental digital content is available for this article. Direct URL citations appear in the printed text and are provided in the HTML and PDF versions of this article on the journal's Web site (www.painjournalonline.com).

Conflict of interest statement

R. Khanna, M. Khanna, and V. Gokhale have filed a provisional patent on the use of quinazoline analogs. The remaining authors have no conflicts of interest to declare.

Appendix A. Supplemental digital content

Supplemental digital content associated with this article can be found online at http://links.lww.com/PAIN/A760.

Inhibition of voltage-gated calcium (CaV) channels is a potential therapy for many neurological diseases including chronic pain. Neuronal CaV1/CaV2 channels are composed of α, β, γ and α2δ subunits. The β subunits of CaV channels are cytoplasmic proteins that increase the surface expression of the pore-forming α subunit of CaV. We targeted the high-affinity protein–protein interface of CaVβ's pocket within the CaVα subunit. Structure-based virtual screening of 50,000 small molecule library docked to the β subunit led to the identification of 2-(3,5-dimethylisoxazol-4-yl)-N-((4-((3-phenylpropyl)amino)quinazolin-2-yl)methyl)acetamide (*IPPQ*). This small molecule bound to CaVβ and inhibited its coupling with N-type voltage-gated calcium (CaV2.2) channels, leading to a reduction in CaV2.2 currents in rat dorsal root ganglion sensory neurons, decreased presynaptic localization of CaV2.2 in vivo, decreased frequency of spontaneous excitatory postsynaptic potentials and miniature excitatory postsynaptic potentials, and inhibited release of the nociceptive neurotransmitter calcitonin gene–related peptide from spinal cord. *IPPQ* did not target opioid receptors nor did it engage inhibitory G protein–coupled receptor signaling. *IPPQ* was antinociceptive in naive animals and reversed allodynia and hyperalgesia in models of acute (postsurgical) and neuropathic (spinal nerve ligation, chemotherapy- and gp120-induced peripheral neuropathy, and genome-edited neuropathy) pain. *IPPQ* did not cause akinesia or motor impairment, a common adverse effect of CaV2.2 targeting drugs, when injected into the brain. *IPPQ*, a quinazoline analog, represents a novel class of CaV2.2-targeting compounds that may serve as probes to interrogate CaVα–CaVβ function and ultimately be developed as a nonopioid therapeutic for chronic pain.

Keywords

CaV2.2; CaVbeta; Specific inhibitor; Rational design; Pain; Trafficking; In silico docking

1. Introduction

The N-type voltage-gated calcium (CaV2.2) channels are critical determinants of increased neuronal excitability and neurotransmission accompanying persistent neuropathic pain.[9,13,18,94] Expressed in the presynaptic termini of primary afferent nociceptors in the spinal cord,[83] CaV2.2 represent a control point for synaptic activity. The potential of targeting CaV2.2 has been demonstrated with attenuation of allodynia by CaV2.2-blocking conotoxins[72] and the altered pain behavior of CaV2.2 knock-out mice.[39,40] CaV2.2 remains a high-value target with several companies developing CaV2.2-targeted compounds.[42,93] Ziconotide (primary alternative to morphine [Prialt])[47] and gabapentin (Neurontin) directly target different elements of the CaV2.2 complex. These drugs, however, present with problematic side effects, difficult dosing regimens, and have high number needed to treat values.[25] Therefore, the development of novel CaV2.2-targeted drugs with improved efficacy and therapeutic index is highly desirable.[65] We have advanced a strategy targeting protein interactions that modulate CaV2.2 as an alternative to direct channel blockade.[11,23,26,85,87] Targeting *channel regulation* may potentially lessen many of the adverse side effects associated with *direct* channel block. Supporting this concept, we reported that targeting CaV2.2 *indirectly* with the CBD3 peptide derived from an ancillary regulatory protein (collapsin response mediator protein 2) did not affect memory

retrieval, motor coordination, and depression-associated behaviors[11] and was not rewarding/addictive.[26]

Here, we focused on the β subunits of voltage-gated calcium (CaV) channels. CaVβs are cytoplasmic proteins encoded by 4 different genes (β_{1-4}), including multiple splice variants.[22] Their signature functions are to increase the surface expression of the pore-forming α subunit of Ca^{2+} channels[22,68] and regulate biophysical properties of the α subunit of Ca^{2+} channels.[22,68] The sum effect of these ancillary roles is to increase the amount of Ca^{2+} influx within cells. In neurons, Ca^{2+} influx triggers neurotransmitter release, where the amount of transmitter released from a presynaptic terminal is dependent on the amount of Ca^{2+} entering the terminal.[4,70] Further involvement of β subunits in regulating synaptic transmission is also supported by evidence of protein–protein interactions of the CaVβ subunits with the synaptic vesicle release machinery.[81] Thus, the subunit is part of the transmitter release site core complex, at the center of which resides the α subunit of the Ca^{2+} channel.[38] Altered CaVβ subunit expression will modulate the function of the α subunit of the calcium channel and can underlie pathological neuronal transmission. In neuropathic pain, CaVβ3 expression is increased and leads to augmented high-voltage-gated Ca^{2+} channel function in small diameter sensory neurons.[43] This pathological increase of CaVβ3 amplifies spinal nociceptive neurotransmission and is sufficient to induce pain.[43] Thus, pharmacotherapeutic approaches targeting the CaVβ–CaVα interface could restore physiological Ca^{2+} homeostasis and be beneficial for chronic pain management.

We used a computational approach to target a protein–protein interface important for voltage-gated calcium channel activity. We report the identification of the small molecule 2-(3,5-dimethylisoxazol-4-yl)-N-((4-((3-phenylpropyl)amino)quinazolin-2-yl)methyl)acetamide (*IPPQ*) targeting the CaVβ–CaVα interface. Here, we demonstrate that *IPPQ* (1) specifically inhibits CaV2.2 (over other subtypes) in sensory neurons, (2) acts at presynaptic sites, (3) blunts release of the pronociceptive neurotransmitter calcitonin gene–related peptide (CGRP), (4) reverses thermal hyperalgesia and mechanical allodynia in acute and neuropathic models of pain, and (5) has no effect on motor activity. This quinazoline analog may be used to mitigate chronic pain by controlling CaV2.2 function.

2. Materials and methods

2.1. Animals and reagents

Adult male Sprague–Dawley rats (225–250 g; Envigo, Indianapolis, IN) were housed in a pathogen-free environment under controlled temperature (23 ± 3°C) and light (12-hour light/12-hour dark cycle; lights on 07:00–19:00) conditions with standard rodent chow and water available ad libitum. All experiments were approved by the Institutional Animal Care and Use Committee (IACUC) of the College of Medicine at the University of Arizona. Procedures were conducted in compliance with the Guide for Care and Use of Laboratory Animals published by the National Institutes of Health and the ethical guidelines of the International Association for the Study of Pain. Animals were randomly assigned to the experimental groups, and treatments and experimenters were blinded to that information. Unless otherwise stated, reagents were purchased from Sigma (St. Louis, MO).

2.2. In silico docking and software for structural representation

Virtual screening workflow was performed in Schrodinger Glide molecular modeling software using the X-ray crystal structure of the complex between CaVβ2a subunit and a peptide of the α1c subunit (PDB code:1 T0J).[79] The α1c subunit peptide was removed, and its binding site was used for docking of 50,000 drug-like small molecule library (molecular weight ≤ 500 Da) available from ChemBridge Inc. The resulting complexes were ranked using Glide XP score and other energy-related terms. Forty-nine compounds were analyzed for their binding in the α-binding pocket on CaVβ2a. Selected compounds were purchased and tested for activity.

2.3. Protein purification

Codon optimized sequence (*Escherichia coli*) for CaVβ2a residues 203 to 425 was inserted between the restriction sites EcoRI-SalI in pET-28a(+) plasmid (synthesized by Genscript). BL21 cells expressing CaVβ2a were resuspended in 50-mM sodium phosphate pH 7.5, 500-mM NaCl, 10% glycerol, supplemented with complete EDTA-free protease inhibitors (Roche, Basel, Switzerland). Disruption of the bacteria was performed by 2 rounds of high-pressure homogenization at 10,000 PSI with a LM10 microfluidizer (Microfluidics, Westwood, MA), and the lysate was centrifuged 45 minutes at 15,000*g* at 4°C. The supernatant was loaded on a His-Trap column (GE Healthcare, Uppsala, Sweden) equilibrated with 50-mM HEPES pH 7.5, 10-mM imidazole, 500-mM NaCl, 10% glycerol, 0.5-mM DTT. After a washing step with 50-mM HEPES pH 7.5, 50-mM imidazole, 500-mM NaCl, 10% glycerol, 0.5-mM DTT, CaVβ2a was eluted with a gradient of imidazole. The fractions of interest were loaded on a HiLoad Superdex size exclusion column (GE Healthcare, Chicago, IL) and eluted with a gradient of imidazole. A Pierce assay was used to determine protein concentration using bovine serum albumin as standard. Protein purity was confirmed with SDS-PAGE. The proteins were flash frozen in liquid nitrogen and stored at −80°C.

2.4. Saturation transfer difference nuclear magnetic resonance spectroscopy

One-dimensional ^{1}H STD NMR[50] for *IPPQ* (1 mM in 100-mM sodium phosphate pH 6.9, 10% D_2O) in the absence of protein was acquired at 25°C on a Varian Inova 600-MHz spectrometer equipped with a Varian cold TR/PFG probe. 1D ^{1}H saturation transfer difference nuclear magnetic resonance (STD NMR)[49] spectra with a spectral width of 12 ppm were collected for samples containing 100-μM *IPPQ* and CaVβ2a in phosphate buffer. Saturation transfer difference nuclear magnetic resonance spectra were collected with a spectral width of 12 ppm, 16 K data points, and 3-second repetition delay. A saturation of the protein was achieved by a 2-second train of selective 50-ms Gaussian pulses centered at 0.74 ppm (on resonance) and 30 ppm (off resonance). A 20-ms spin lock was used to suppress the protein signal, followed by the double PFG spin echo to remove residual water signal. We acquired 512 scans per experiment. The on-resonance and off-resonance spectra were acquired interleaved, and the difference spectrum was acquired by phase cycling. Spectra processing and analysis were performed with the VNMRJ 3.2 and MestReNova 7.1.

2.5. Microscale thermophoresis

Microscale thermophoresis (MST), a technique monitoring the thermophoretic movement of molecules in optically generated microscopic temperature gradients to allow for analysis of biomolecular interactions was performed as before.[86,87] In MST, increasing concentrations of unlabeled ligand are mixed with the fluorescently labeled biomolecule, kept at constant concentration. Purified Beta2-CaV-His was fluorescently labeled using the His-Tag labeling kit RED-Tris-NTA second generation (Nanotemper, München, Germany) according to the manufacturer's instructions. Briefly, Beta2-CaV-His was diluted to 200 nM in PBS supplemented with 0.1% Tween-20 (PBS-T buffer) and 0.1% PEG 8000 and mixed with one molar equivalent of the fluorescent NT-647-His-labeling dye and incubated for 30 minutes at room temperature. Labeled Beta2-CaV was then centrifuged at 15,000*g* for 10 minutes at 4°C. A total of 25 nM of labeled Beta2-CaV-His protein were mixed with increasing concentrations of AID-CaV2.2 peptide in PBS-T, 0.1% PEG 8000 buffer, and incubated 10 minutes at room temperature. The thermophoresis measurements were performed on a Monolith NT.115 (Nanotemper) using MST premium capillaries, at 100% LED at high MST power. Data analysis was performed with the MO Affinity Analysis software (Nanotemper) using the Kd model (standard fitting model derived from law of mass action).

2.6. Primary cell culture of dorsal root ganglia

Dorsal root ganglion (DRG) from all vertebral levels was harvested and dissociated using methods described previously.[56,59,88] Briefly, DRG were dissected from naive animals and treated with collagenase, type I (5 mg/mL), and neutral protease (3.125 mg/mL) in bicarbonate-free DMEM for 45 minutes (Worthington Biochemical, Lakewood, NJ). Mechanical trituration in culture medium (DMEM with 10% fetal bovine serum, penicillin [100 mg/mL], streptomycin [100 U/mL], normocin [0.8 μg/mL], and nerve growth factor [30 ng/mL], Life Technologies, Carlsbad, CA) was then used to dissociate the cells. The cells were then plated in 20 μL of medium on poly-L-lysine/laminin-coated coverslips (BD bioscience, San Jose, CA) and incubated for up to 2 hours before culture media was added to the wells up to a final volume of 1 mL. The cells were then left undisturbed at 37°C (with 5% CO_2) for 12 to 18 hours to allow adhesion.

2.7. Calcium imaging

Dorsal root ganglion neurons were incubated with 3-μM Fura-AM (Cat#F-1221; Life Technologies, stock solution prepared at 1 mM in DMSO, 0.02% pluronic acid, Cat#P-3000MP; Life Technologies) for 30 minutes at 37°C to allow monitoring of changes in intracellular calcium ($[Ca^{2+}]_c$). Recordings were performed in standard Tyrode's solution (119-mM NaCl, 2.5-mM KCl, 2-mM $MgCl_2$, 2-mM $CaCl_2$, 25-mM Na HEPES, 30-mM glucose, pH 7.4,~310 mOsm) at room temperature (~23°C). A 1-minute baseline was acquired followed by brief stimulations (15 seconds) either with a solution (81.5-mM NaCl, 40-mM KCl, 2-mM $CaCl_2$, 2-Mm $MgCl_2$, 25-mM HEPES, 30-mM glucose, pH 7.4, ~310 mOsm) to activate low-voltage-activated Ca^{2+} channels (ie, T-type Ca^{2+} channels [CaV3.1-CaV3.3] and R-type [CaV2.3]), or a solution (32-mM NaCl, 90-mM KCl, 2-mM $MgCl_2$, 2-mM $CaCl_2$, 25-mM HEPES, 30-mM glucose, pH 7.4, ~310 mOsm) to activate high-voltage-activated Ca^{2+} channels (ie, P/Q-type [CaV2.1], R-type [CaV2.3], N-type [CaV2.2], and L-

type [CaV1.1-CaV1.4]). Acquisition was performed using an Nikon Eclipse T*i*-U (Melville, NY) inverted microscope, equipped with an objective photometrics-cooled CCD camera CoolSNAP ES^2 (Roper Scientific, Tucson, AZ) and a Nikon Super Fluor ×10 0.50 objective and operated by the NIS Elements software (version 4.20; Nikon Instruments, Melville, NY). The excitation light was delivered by a Lambda-LS system (Sutter Instruments, Novato, CA). The excitation filters (340 ± 5 and 380 ± 7 nm) were controlled by a Lambda 10 to 2 optical filter change (Sutter Instruments). Fluorescence was recorded through a 505-nm dichroic mirror at 535 ± 25 nm. To reduce photo-bleaching, pictures were taken every ~10 seconds over the duration of the experiment with the minimal exposure time providing sufficient image quality. $[Ca^{2+}]_c$ changes were followed using the F_{340}/F_{380} ratio calculated after background subtraction from both channels. *IPPQ* was applied at 20 μM overnight for the initial screening.

2.8. Constellation pharmacology

Constellation pharmacology[56,75,76,88] was performed as described in 2.7, but after baseline recording in Tyrode's solution, DRG neurons were sequentially stimulated for 15 seconds using the following receptor agonists: 400-nM menthol, 50-μM histamine, 10-μM adenosine triphosphate (ATP), 200-μM allyl isothiocyanate (AITC), 1-mM acetylcholine (Ach), and 100-nM capsaicin diluted in standard Tyrode's solution. Cells were washed 5 minutes in standard Tyrode's solution between each agonist, and cell viability was assessed by depolarization-induced Ca^{2+} influx using the excitatory solution for activating high-voltage-activated Ca^{2+} channels at the end of the constellation pharmacology recording. Agonist application was automated using the ValveBank Controller (Automate Scientific, San Francisco, CA). A cell was classified as a "responder" if its maximum fluorescence ratio for 340/380 nm exceeded 10% of its baseline value (calculated as the average fluorescence ratio during the 30 seconds immediately preceding application of the receptor agonist solution).

2.9. MOR-CHO, DOR-CHO, and KOR-CHO cell lines and cell culture

The MOR-CHO cell line was obtained from PerkinElmer (#ES-542-C). Creation of the DOR cell line was reported elsewhere.[74] For the KOR cell line, an N-terminal 3X-hemagglutinin tagged human KOR expression clone from Genecopoeia was electro-porated into parental CHO cells and selected with 500-μg/mL G418. KOR-expressing cells were subjected to live cell labeling with anti-HA-Alexa488 antibody and triage of the top 2% of the population by flow cytometry was performed. Characterization was performed using immunocytochemistry and Western blot to verify receptor expression and expected signal transduction activation. All 3 cell lines were characterized by saturation radioligand binding with ^{3}H-diprenorphine. Measured K_D were used in competition binding experiments to calculate the K_I (MOR = 5.23 nM; DOR = 0.93 nM; KOR = 1.81 nM; all the mean of N ≥ 3 independent experiments). Cell cultures was performed 50% DMEM 50% F12 media supplemented with 10% heat-inactivated FBS and 1X penicillin/streptomycin (Gibco; Thermo Fisher) at 37°C with 5% CO_2; propagation cultures were further maintained in 500-μg/mL G418. Cultures were propagated for no more than 20 passages before discarding. Cell pellets for experiments were grown in 15-cm plates and harvested in dPBS (Ca^{2+}- and Mg^{2+}-free) with 5-mM EDTA and stored at −80°C before use.

2.9.1. Competition radioligand binding—Competition radioligand binding experiments were performed as previously reported.[74] Cell membrane preparations of MOR-, DOR-, or KOR-CHO were combined with a constant concentration of ^{3}H-diprenorphine (MOR = 5.33 nM; DOR = 1.43 nM; KOR = 1.95 nM) and a concentration curve of competitor ligand. Reactions were performed in 200 μL in 96 well plates for 60 minutes at room temperature. Termination of the reaction was obtained by rapid filtration through 96-well format GF/B filter plates (PerkinElmer, Waltham, MA) with cold water, washing, drying, adding of, and Microscint PS (PerkinElmer). Plate reading was performed on a MicroBeta2 96 well format 6 detector scintillation counter (PerkinElmer). The data were normalized to the specific binding caused by ^{3}H-diprenorphine alone (100%) or nonspecific binding determined by a 10-μM concentration of known competitor ligand (0%; MOR = naloxone; DOR = SNC80; KOR = naloxone). K_I values were calculated using the IC_{50} of each competitor ligand and the previously established K_D of ^{3}H-diprenorphine in each cell line (GraphPad Prism 7.0).

2.10. Whole-cell voltage-clamp electrophysiology

HEK293 cells and acutely dissociated DRG neurons were used for recordings. Experiments were performed at room temperature by using an EPC10 Amplifier-HEKA. Electrodes were pulled from thin-walled borosilicate glass capillaries (Warner Instruments, Hamden, CT) with a P-97 electrode puller (Sutter Instrument) to reach final electrode resistances of 1 to 3 MΩ when filled with internal solutions. External solution was 140-mM Et_4N $MeSO_3$, 10-mM HEPES, and 5-mM $BaCl_2$ at pH 7.3 and internal solution 135-mM $CsMeSO_3$, 5-mM CsCl, 5-mM EGTA, 1-mM $MgCl_2$, 4-mM MgATP, and 10-mM HEPES at pH 7.3 for HEK293 cells. For DRGs, external solution (at ~315 mOsm, in mM): 10 glucose, 10 HEPES, 10 $BaCl_2$, 30 TEA-Cl, 110 N-methyl-D-glucamine (NMDG) (pH 7.2 with KOH); internal solution: (at ~305 mOsm, in mM): 5 BAPTA, 5 Mg-ATP, 10 HEPES, 150 $CsCl_2$ (pH 7.2 with KOH). Isolation of specific current contributions of each calcium channel subtypes was obtained by treating the cells with inhibitors of all other Ca^{2+} channel subtypes. The following compounds were used: ω-conotoxin GVIA (500 nM, N-type voltage-gated Ca^{2+} channel blocker),[24] SNX482 (200 nM, R-type voltage-gated Ca^{2+} channel blocker),[62] ω-agatoxin (200 nM, P/Q-type voltage-gated Ca^{2+} channel blocker),[52] nifedipine (10 μM, L-type voltage-gated Ca^{2+} channel blocker), and TTA-P2 (1 μM, T-type voltage-gated Ca^{2+} channel blocker).[17] Cells were subjected to current–voltage, inactivation, and use dependence protocols.

2.10.1. Voltage-clamp protocols—Ca^{2+} channel activation was analyzed as a function of current vs voltage, and peak current density was recorded, typically near ~0 to 10 mV. In the current-voltage protocol, DRG neurons were held at resting membrane potential for 5 ms before depolarization by 200-ms voltage steps from −70 mV to +60 mV in 10-mV increments. Normalization of currents to each cell's capacitance (pF) was performed to allow for collection of current density data to analyze activation of Ca^{2+} channels as a function of current vs voltage as well as peak current density. Dorsal root ganglion neurons were held at −90 mV for 20 ms for the inactivation protocol before depolarizating by 1.5-second voltage steps from −100 to +10 mV in 10-mV increments, followed by a 20-ms pulse at 10 mV before returning to −90 mV for 20 ms. For the use dependence protocol,

DRGs were submitted 30 times to this protocol: baseline held at −70 mV for 5 ms before depolarization to 0-mV voltage step lasting 200 ms and followed by a return to −70 mV for 5 ms.

2.11. Preparation of spinal cord slices

Young rats (12–21 days postnatal) were deeply anesthetized using isoflurane, as described previously.[96] For spinal nerve blocking, 2% lidocaine in a final volume 0.3 mL was injected to both sides of lumbar vertebrae L4 to 5. Laminectomy was performed from midthoracic to low lumbar levels. The spinal cord was harvested and placed in chilled modified artificial cerebrospinal fluid (80-mM NaCl, 2.5-mM KCl, 1.25-mM NaH_2PO_4, 0.5-mM $CaCl_2$, 3.5-mM $MgCl_2$, 25-mM $NaHCO_3$, 75-mM sucrose, 1.3-mM ascorbate, 3.0-mM sodium pyruvate, pH 7.4, ~310 mOsm) oxygenated with 95% O_2 and 5% CO_2. Transverse 350-mm-thick slices were cut on a vibratome (VT1200S; Leica, Nussloch, Germany). Slices were then placed in an oxygenated recording solution (125-mM NaCl, 2.5-mM KCl, 2-mM $CaCl_2$, 1-mM $MgCl_2$, 1.25-mM NaH_2PO_4, 26-mM $NaHCO_3$, 25-mM D-glucose, 1.3-mM ascorbate, 3.0-mM sodium pyruvate, pH 7.4, ~320 mOsm) for at least 1 hour at RT. The slices were then positioned in the recording chamber and with continuous perfusion of oxygenated recording solution at 3 to 4 mL/minute before electrophysiological recordings at RT.

2.11.1. Electrophysiological recording in spinal cord slices by whole-cell patch clamp—

Substantia gelatinosa neurons were identified in the slices with an infrared differential interference contrast video microscopy on an upright microscope (FN1; Nikon, Tokyo, Japan) equipped with a 3 40/0.80 water-immersion objective and a CCD camera. Electrodes were obtained by pulling thin-walled borosilicate glass capillaries (Warner Instruments) with a P-97 electrode puller (Sutter Instrument) to reach a final electrode resistances of 6 to 10 MΩ when filled with potassium gluconate–based internal solutions (120-mM potassium gluconate, 20-mM KCl, 2-mM $MgCl^2$, 2-mM Na2-ATP, 0.5-mM Na-GTP, 20-mM HEPES, 0.5-mM EGTA, pH 7.28, ~310 mOsm). Membrane potential was held at −60 mV using PatchMaster software and a dual channel EPC10-HEKA amplifier (Lambrecht, Germany).

A giga-ohm seal was then formed, and whole-cell configuration was obtained in voltage-clamp mode. To record spontaneous excitatory postsynaptic currents (sEPSCs), bicuculline methiodide (10 μM) and strychnine (1 μM) were added to the recording solution to block γ-aminobutyric acid–activated and glycine-activated currents. To record miniature EPSCs (mEPSCs), tetrodotoxin (TTX, 1 μM) was also added to the recording solution to block the action potentials. Hyperpolarizing step pulses (5 mV in intensity, 50 ms in duration) were periodically delivered to monitor the series resistance (15–25 MΩ), and recordings were discontinued if the series resistance changed by more than 20%. For each neuron, sEPSCs and mEPSCs were recorded for a total duration of 2 minutes. Drugs were dissolved in artificial cerebrospinal fluid or 0.1% DMSO, and the solution was applied through perfusion. The recordings were obtained within 30 minutes to 3 hours of drug perfusion; no difference was observed between recordings performed earlier vs later in the window after drug perfusion (data not shown). Currents were filtered at 3 kHz and digitized at 5 kHz.

Data were further analyzed by the Mini-Analysis Program (Synatosoft Inc, Decatur, GA) to provide spreadsheets for the generation of cumulative probability plots. The amplitude and frequency of sEPSCs and mEPSCs were compared between neurons from animals in control and *IPPQ* groups.

2.12. Calcitonin gene–related peptide release from lumbar slices

Rats were placed under deep anesthesia with 5% isofluorane and then decapitated. Cervical and lumbar incisions were made to expose the spinal cord. Hydraulic pression was applied with a saline-filled syringe inserted into the lumbar vertebral foramen to extrude the spinal cord. The lumbar region was cut for use in the CGRP release assay. Baseline treatments (#1 and #2) consisted of bathing in Tyrode's solution. A total of 90-mM KCl were used for excitatory solution (as in calcium imaging experiments) and were paired with the treatment for fraction #4. Four hundred–microliter fractions were collected every 10 minutes for CGRP release measurements. Samples were flash frozen and stored at −20°C. *IPPQ* (20 μM) or vehicle (0.9% saline) was added to the pretreatment and cotreatment fractions (#3 and 4) for 10 minutes. Enzyme-linked immunosorbent assay (Cat# 589001, Cayman Chemical, Ann Arbor, MI) was used to determine the concentration of CGRP released in the buffer.

2.13. Synapse enrichment and fractionation

Adult rats were anesthesized using isoflurane and decapitated. Spinal cords were removed, and the dorsal horn of the spinal cord was dissected because this structure contains the synapses arising from the DRG. Synaptosomes isolation was performed as described previously.[64] Fresh tissues were homogenized in ice-cold sucrose 0.32 M, HEPES 10 mM, pH 7.4 buffer. Insoluble material was pelleted by centrifugation at 1000*g* for 10 minutes. The supernatant was collected and centrifuged at 12000*g* for 20 minutes to pellet a crude membrane fraction. The membrane fraction was resuspended in a hypotonic buffer (4-mM HEPES, 1-mM EDTA, pH 7.4). Resulting synaptosomes were pelleted by centrifugation at 12000×g for 20 minutes and incubated in 20-mM HEPES, 100-mM NaCl, 0.5% triton X, pH 7.2) for 15 minutes and centrifuged at 12000*g* for 20 minutes. Sample incubations were performed on ice, and all centrifugations were performed at 4°C. Non-postsynaptic density (non-PSD) membrane fraction, sometimes referred to as the triton-soluble fraction, was obtained from the supernatant. The pellet containing the PSD fraction was solubilized in RIPA buffer (50-mM Tris-HCl, pH 7.4, 50-mM NaCl, 2-mM $MgCl_2$, 1% [vol/vol] NP40, 0.5% [mass/vol] sodium deoxycholate, 0.1% [mass/vol] SDS) as described previously.[26] All buffers were supplemented with phosphatase inhibitors (Cat# B15002, Bimake) and protease inhibitors (Cat# B14002; Bimake, Houston, TX). Non-PSD and PSD fraction's integrity was verified by immunoblotting. PSD95 was enriched in the PSD fractions while synaptophysin was enriched in non-PSD fractions. BCA protein assay was used to determine protein concentrations.

2.14. Immunoblot preparation and analysis

Indicated samples were loaded on 4% to 20% Novex gels (Cat# EC60285BOX; Thermo Fisher Scientific, Waltham, MA). Proteins were transferred at 120 V for 1 hour using TGS buffer (25-mM Tris pH = 8.5, 192-mM glycine, 0.1% (mass/vol) SDS), 20% (vol/vol) methanol as transfer buffer to 0.45-μm polyvinylidene difluoride membranes (Cat#

IPVH00010; Millipore, Billerica, MA), preactivated in 100% methanol. A blocking step was then performed in TBST (50-mM Tris-HCl, pH 7.4, 150-mM NaCl, 0.1% Tween 20), 5% (mass/vol) nonfat dry milk for 1 hour at room temperature, then incubated separately with primary antibodies: CaV2.2 (Cat# TA308673; Origene, Rockville, MD), PSD95 (Cat# MA1–045, Thermo Fisher scientific), synaptophysin (Cat# MAB5258, Thermo Fisher scientific, San Diego, CA), or flotillin (Cat# F1180; Sigma, St. Louis, MO) in TBST, 5% (mass/vol) BSA, at 4°C overnight. After incubation in horseradish peroxidase–conjugated (HRP) secondary antibodies (Jackson Labs) revelation was performed using enhanced luminescence (WBKLS0500; Millipore) before exposure to photographic film. Films were scanned and quantified using Un-Scan-It gel scanning software (version 6.1; Silk Scientific Inc).

2.15. Indwelling intrathecal catheter

Rats were anesthetized with ketamine/xylazine 80/12 mg/kg intraperitoneally (i.p.) (Sigma), and their head was placed in a stereotaxic frame. The cisterna magna was exposed and incised. As previously reported, an 8-cm catheter (PE-10; Stoelting, Wood Dale, IL) was implanted, terminating in the lumbar region of the spinal cord.[89] Catheters were sutured (using 3–0 silk sutures) into the deep muscle and externalized at the back of the neck. Autoclips were used to close the skin, and other surgeries were performed after a 5- to 7-day recovery period.

2.16. Behavioral measurements

2.16.1. Measurement of thermal withdrawal latency—The method of Hargeaves was used. Rats, either naive or after experimentally induced pain (see below), were acclimated to plastic boxes placed on a clear glass plate maintained at 30°C. As per the Hargreaves et al.[28] method, a radiant heat source (high-intensity projector lamp) was focused onto the hind-paw plantar surface. When the paw was withdrawn, a motion detector halted the stimulus and recorded the time. A 33.5-second maximal cutoff was used to avoid tissue damage.

2.16.2. Measurement of allodynia—Tactile allodynia (ie, a decreased threshold to paw withdrawal after probing with normally innocuous mechanical stimuli) was assessed by measuring rats' paw withdrawal threshold in response to probing with a series of fine calibrated filaments (von Frey). Rats were placed in suspended plastic cages with wire mesh floor, and each von Frey filament was applied perpendicularly to the plantar surface of the paw. The "up-and-down" method (sequential increase and decrease of the stimulus strength) was used to determine the withdrawal threshold Dixon's nonparametric method was used for data analysis, as described by Chaplan et al.[15,21] Data were expressed as the mean withdrawal threshold.

2.17. Pain models

2.17.1. Paw incision model of postoperative pain—A rodent model of surgical pain was generated by plantar incision as previously described.[10] Male rats (Sprague–Dawley) were anesthetized with gas isoflurane. The plantar side of the left hind paw was scrubbed 3 times with betadine followed by 70% alcohol. A 1-cm-long incision, starting

0.5 cm from the heel and extending toward the toes, was made using a number 11 blade. Incision cut through the skin and fascia of the plantar aspect of the hind paw, including the underlying muscle. A longitudinal incision was made in the plantaris muscle leaving both muscle origin and insertion intact. Gentle pressure was applied to facilitate hemostasis, and the skin was closed with 2 mattress sutures using 5–0 nylon attached to a curved needle. Rats were injected with gentamicin (8 mg/kg, subcutaneously) and were allowed to recover from anesthesia before being returned to their home cage. Sham rats were anesthetized, and the left hind paw was scrubbed as previously described, but no incision was made. After surgery, rodents were allowed to recover for 24 hours before measurements of paw withdrawal thresholds and paw withdrawal latencies.

2.17.2. Spinal nerve ligation model of neuropathic pain—Nerve ligation injury induces signs of neuropathic dysesthesias that include thermal hypersensitivity and tactile allodynia. Nerve operations were performed 5 days after intrathecal catheter implantation. After anesthesia with 2% isoflurane in O_2 at 2 L/minute, the skin over the caudal lumbar region was incised, and the muscles retracted. Spinal nerves located at L5 and L6 were exposed and carefully isolated. A tight nerve ligation with 4–0 silk was placed distal to DRG without limiting the use of the left hind paw of the animal. All animals were given 7 days to recover before any testing. Any animal exhibiting signs of motor deficiency was euthanized.

2.17.3. Elevated plus maze test of anxiety-related behaviors—One hour after i.p. injection of *IPPQ* or its vehicle, mice (CD1) were placed at the center of the elevated plus maze, where the 2 arms intersect and allowed to explore the maze freely for 10 minutes. The apparatus dimensions were as follows: arm length: 35 cm; arm width: 5 cm; and wall height for closed walls: 15 cm. The whole apparatus is elevated 50 cm above ground. Animals movements were recorded by a camera (C310; Logitech, Lausanne, Switzerland) placed above the apparatus and tracked and analyzed using the Any-MAZE software (v6.05; Stoelting). Entry into a zone was defined as 70% of the animal's body being in the zone. The main parameter analyzed was the time spent into the open arms of the apparatus.

2.17.4. Acute pain models—The tail flick response was evoked either by a light beam (irradiated heat) or by immersion of one-third of the tail in water warmed at 52°C. For the hot-plate test, mice were placed on a metal plate (52°C), and a timer was started. Timer was stopped after the first positive response: jumping, hind paw licking, or hind paw flinching. A 10-second cutoff time was used for tail-flick tests, and a 20-second cutoff time was used for hot-plate test.

2.17.5. HIV-induced sensory neuropathy—A model of HIV-induced sensory neuropathy was produced by intrathecal (i.t.) administration of the glycoprotein $gp120^{51}$ from the HIV-1 envelope. Baseline behavioral measurements were obtained 7 days after implantation of an i.t. catheter. Rats were then randomly assigned to 2 groups, treated of vehicle. On days 10, 12, and 14, rats were injected i.t. with either 300 ng of gp120 (Cat#4961, HIV-1 BaL gp120 recombinant protein, NIH-AIDS Reagent program) in a final volume of 20 μL in 0.9% saline and 0.1% BSA or vehicle alone.

2.17.6. Chemotherapy-induced peripheral neuropathy through paclitaxel—

Rats were administered pharmaceutical-grade paclitaxel (Cat# P-925–1; Goldbio, Olivette, MO) resuspended at a concentration of 2 mg/mL in 30% 1:1 Cremophor EL: ethanol, 70% saline at 2 mg/kg i.p.. Based on the protocol described by Polomano et al.,[66] injection were repeated every other day for a total of 4 injections (days 0, 2, 4, and 6), resulting in a final cumulative dose of 8 mg/kg. Animals developed mechanical hyperalgesia within 10 days after the first injection. No abnormal spontaneous behavioral changes in the rats were noted during or after the treatment.

2.17.7. In vivo transfection of CRISPR plasmids for Cas9-mediated editing of Nf1—

As described before,[55,58,60] NF1-related pain was induced by CRISPR-/Cas9-mediated editing of the exon 39 of the gene *Nf1*. The specific gRNA sequence was cloned in the plasmid pLCRISPR-EFS-tRFP[29] and was validated in Ref. 55. Lentiviral particle were produced by Viracore (UCSF) and provided concentrated at a titer higher than 10^7 infectious particles per ml. At day 0, 5 μL of the lentiviral concentrate was injected intrathecally in male Sprague–Dawley rats. After 10 days, rats developed thermal hyperalgesia as described before.[55,58,60]

2.18. Rotarod

Rats were trained to walk on a rotating rod (10 rev/minute; Rotamex 4/8 device) with a maximal cutoff time of 180 seconds. Training was initiated by placing the rats on a rotating rod and allowing them to walk until they either fell off or 180 seconds was reached. This process was repeated 6 times. Before treatment (intracerebroventricular [i.c.v.] injection of *IPPQ* or saline), the rats were run once on a moving rod to establish a baseline value. Assessment consisted of placing the rats on the moving rod and timing until either they fell off or reached a maximum of 180 seconds.

2.19. Statistics

Statistical analyses were performed using GraphPad Prism 7 (GraphPad, La Jolla, CA). Unless stated otherwise, data were obtained from a minimum of 6 independent biological replicates. All data represent the mean ± SEM. The statistical significance of differences between mean values was calculated using either parametric or nonparametric Student *t* test, analysis of variance followed by post hoc comparisons (Tukey) using GraphPad Prism 7. To determine the type of test to use, all data were first tested for a Gaussian distribution using a D'agostino–Pearson test (GraphPad Prism 7 Software). Statistical significance threshold was set at $\alpha < 0.05$.

3. Results

3.1. A quinazoline compound (*IPPQ*) targets the CaVα–CaVβ interface and inhibits depolarization-evoked Ca^{2+} influx in sensory neuron subpopulations

To identify small molecules that disrupt the CaVα–CaVβ interaction, we used a virtual screening approach against the crystal structure of the complex formed between the CaVβ2a subunit and a peptide of the α1c subunit (Fig. 1A).[79] The alpha-interaction domain (AID) peptide was removed, and its binding site was used for docking 50,000 drug-like small

molecules (molecular weight ≤ 500 Da) commercially available from ChemBridge Inc. The resulting complexes were ranked using Glide score and other energy-related terms.[27] Forty-nine compounds docked into the α-binding pocket on CaVβ2a. The 49 compounds were screened by Ca^{2+} imaging for their ability to inhibit depolarization-induced calcium influx in rat DRG neurons. Of these compounds, 13 were either insoluble or killed the neurons, and 11 compounds inhibited Ca^{2+} influx by ≥50%. One docked compound, *IPPQ*, engaged all 3 (V241, I343, and N390) AID "hotspot" residues (Fig. 1B). The structure of *IPPQ* aligned with 3 residues (W440, I441, and Y437) from the AID (Figs. 1C and E) and specifically bound CaVβ2a protein in saturation transfer difference nuclear magnetic resonance (STD-NMR) (Fig. 1D).

Microscale thermophoresis—a method that permits analysis of biomolecular interactions—demonstrated that *IPPQ* reduced the binding of CaVβ2-His to the AID-CaV2.2 peptide from a K_d of 12 to 208 nM (Fig. 1F), reduced the binding of CaVβ2-His to the AID-CaV2.1 peptide from a K_d of 18.3 to 93 nM (Fig. 1G), and reduced the binding of CaVβ2-His to the AID-CaV1.1 peptide from a K_d of 24 nM to 51 nM (Fig. 1H) while binding of CaVβ2-His to the AID peptides from CaV1.2/CaV1.3/CaV1.4 (Fig. 1I) and CaV2.3 (Fig. 1J) was unaffected. Whether the inhibition was achieved through *IPPQ* binding to the predicted pocket on CaVβ or through allosteric modulation remains to be determined.

IPPQ inhibited depolarization-evoked Ca^{2+} influx in a concentration-dependent manner in DRG sensory neurons with an IC_{50} of ~9.1 μM (Fig. 1K). Since compounds are known to aggregate at screening-relevant concentrations in every compound library, we queried the Aggregator Advisor database[19] with *IPPQ*, which revealed no similarity to known aggregators. A similar query of *IPPQ* in the Zinc15 database revealed no hits to molecules containing PAINS chemotypes. As the Aggregator Advisor calculated a partition coefficient for *IPPQ* in n-octanol/water (cLogP) value of 3.5, which is in the range reported for many other aggregators,[35] dynamic light scattering was performed. Dynamic light scattering curve of *IPPQ* in the presence of a nonionic detergent (0.1% Tween-20) did not reveal significant colloidal aggregation with only less than 9% of the compound forming particles around a 50-nm radius (supplementary Fig. 1A, available at http://links.lww.com/PAIN/A760). To further control for potential effects of aggregation, we subjected *IPPQ* to a centrifugation step (15 minutes at 21,000*g*) and then used the supernatant from the spin-down of *IPPQ* to perform calcium imaging studies in sensory neurons. There were no differences in the depolarization-triggered calcium responses between cells treated with *IPPQ* irrespective of whether it was centrifuged or not (supplementary Fig. 1B, available at http://links.lww.com/PAIN/A760). These data, along with the use of nonionic detergent in the MST experiments (Figs. 1F–J) and Tween-80 in the vehicle for all in vivo experiments, triangulate to eliminate colloidal aggregation as a mechanism of *IPPQ*'s inhibitory effect.

Next, we assessed whether Ca^{2+} influx was inhibited by *IPPQ* in all classes of DRG neurons (Figs. 2A–D), identified by constellation pharmacology—a method that permits functional "fingerprinting" of neurons to specific receptor agonists.[76] Sensory neurons were treated with 20 μM of *IPPQ* and then stimulated with specific receptor agonists allowing us to identify different functional populations of sensory neurons (Figs. 2A–B). *IPPQ* treatment increased the functional capacity of sensory neurons because they were able to respond to

more receptor agonists than vehicle-treated neurons (Fig. 2A). This was correlated with an increased number of neurons responding to ATP and histamine (Fig. 2B). *IPPQ* decreased the peak response elicited by each receptor agonist (Fig. 2C). Depolarization-evoked Ca^{2+} influx was inhibited by *IPPQ* in all DRG sensory neuron functional classes (Fig. 2D). These results show that targeting the CaVβ–CaVα interface using *IPPQ* decreases voltage-gated Ca^{2+} channel activity across a functionally heterogenous sensory neuron subpopulation.

3.2. Preferential activity of *IPPQ* for CaV2.2

Because the CaVα–CaVβ pocket is conserved across the various α and β subunits, we next set out to determine whether *IPPQ* was selective for any of the isoforms. We began with a heterologous system (human embryonic kidney 293 [HEK293] cells) wherein precise control of subunits could be achieved. Here, we expressed the α subunit of CaV2.2 in combination with CaVβ1–4 subunits in heterologous cells and measured whole cell currents. *IPPQ* inhibited CaV2.2 currents when coexpressed with CaVβ subunits 1 to 3 (Figs. 3A–D), but not with CaVβ4 (Fig. 3E). The presence of α2δ−1 did not affect the inhibition conferred by *IPPQ* (Figs. 3C and D). Together, these results demonstrate selectivity of *IPPQ* for N-type channels with CaVβ subunits 1 to 3, but not CaVβ4.

Next, using whole-cell patch-clamp electrophysiology, we measured Ca^{2+} currents in DRG neurons treated overnight (15–18 hours) with 20 μM of *IPPQ* (~twice the IC_{50} of ~9.1 μM) or 0.1% DMSO as a control (Fig. 4A). Consistent with our Ca^{2+} screening, *IPPQ* inhibited (by ~50%) total Ca^{2+} currents in DRG sensory neurons (Figs. 4B and C), without affecting the biophysical properties (activation and inactivation) of these channels (Figs. 4D and E). Next, using saturating concentrations of selective Ca^{2+} channel inhibitors, we isolated either CaV1 (L-type), CaV2.1 (P/Q-type), CaV2.2 (N-type), or CaV2.3 (R-type) Ca^{2+} currents in DRGs to evaluate the inhibitory potential of *IPPQ* on each subtype. *IPPQ* (20 μM) inhibited only N-type Ca^{2+} channels (>70%) but had no effect on the other subtypes (Fig. 4F).

3.3. Lack of activity of *IPPQ* for opioid receptors

Inhibition of Ca^{2+} influx in sensory neurons can occur through activation of opioid receptors.[36] Consequently, we tested whether opioid receptors could be engaged by *IPPQ* by competition radioligand binding at all 3 opioid receptors in vitro. We competed *IPPQ* and a positive control compound (naloxone for MOR and DOR, U50488 for KOR) vs a fixed concentration of ^{3}H-diprenorphine in Chinese hamster ovary (CHO) cells expressing the human μ (MOR), δ (DOR), or κ (KOR) opioid receptor. *IPPQ* (up to 10 μM) did not bind to the MOR or KOR and only bound to the DOR with very weak affinity (Figs. 5A–C). By contrast, the positive control compounds bound to all 3 targets with expected affinity (Figs. 5A–C). Thus, inhibition of Ca^{2+} influx by *IPPQ* likely does not involve opioid receptors. Compound *IPPQ* was evaluated at UNC's NIMH Psychoactive Drug Screening Program against a battery of 30 receptors known to adversely impact drug effectiveness. No significant binding was observed at 20 μM. Moreover, *IPPQ* did not affect hERG K^{+} channel activity at 20 μM, which helps to confirm drug safety (data not shown).

CaV2.2 function can be regulated by the G protein–coupled receptor (GPCR) Gi signaling after activation of the μ opioid or the GABA-B receptors.[1] To test whether *IPPQ*-mediated

inhibition of CaV2.2 could involve Gi-coupled GPCR signaling, we used the prepulse facilitation electrophysiological protocol that relies on applying strong depolarizing prepulse to dissociate the interaction between CaV2.2 and the Gβγ subunits.[95] This triggers a relief of GPCR-mediated inhibition of the calcium channel and allows for a second recording of calcium currents. We did not find any evidence of GPCR-mediated inhibition of CaV2.2 with *IPPQ* (Figs. 5D and E) thus rejecting the hypothesis that *IPPQ* acts through activating any inhibitory GPCR signaling. Norepinephrine (NE) was chosen as a control because it has been demonstrated to inhibit Ca^{2+} currents in a voltage-dependent manner.[34,78]

3.4. *IPPQ* inhibits spinal neurotransmission

CaV2.2 is involved in spinal nociceptive neurotransmission[30] through the control of presynaptic nociceptive neurotransmitter release from C fibers.[11,30,59,73] *IPPQ*-mediated inhibition of CaV2.2 from DRG neurons should in turn decrease spontaneous excitatory postsynaptic currents (sEPSCs) measured in the *substantia gelatinosa* of the dorsal horn of the spinal cord. We recorded sEPSCs from neurons in laminae I-II in this region of the lumbar dorsal horn (Fig. 6A). *IPPQ* treatment had no effect on the amplitude of the recorded sEPSCs (Figs. 6C and D). However, we observed a decrease of sEPSC frequency after treatment with 20 μM of *IPPQ* (Figs. 6E and F). We next investigated the effects of *IPPQ* (20 μM) on miniature EPSCs (mEPSCs) and found that both the frequency and amplitude of mEPSCs were decreased (Figs. 6G–J).

To determine whether the actions of *IPPQ* were presynaptic or postsynaptic, we also analyzed EPSCs evoked by a paired-pulse stimulation protocol, which is commonly used to assess changes in presynaptic function.[97,98] At 50-ms intervals, paired-pulse ratios were increased by *IPPQ* (20 μM) treatment (Figs. 7A and B). These results collectively implicate a presynaptic provenance for the mechanism of *IPPQ*'s action on spinal synaptic neurotransmission.

3.5. *IPPQ* reduces CaV2.2 spinal presynaptic localization

IPPQ can inhibit CaV2.2 AID interaction with the beta subunits. We asked whether interfering with this interaction using *IPPQ* in vivo could affect CaV2.2 presynaptic localization in lumbar dorsal horn of the spinal cord. We first extracted synaptosomes from the dorsal horn of the spinal cord of rats 1 hour after injection with *IPPQ* (2 μg in 5 μL, intrathecally) and isolated before and after synaptic fractions (Fig. 8A). The fractionation efficiency was verified by western blot where the postsynaptic marker PSD95 was highly enriched in the PSD fraction, whereas the presynaptic marker synaptophysin was only found in the non-PSD fraction (Fig. 8A). Indeed, CaV2.2 was exclusively localized in the presynaptic fraction (Fig. 8A). We then focused on the presynaptic (non-PSD) fraction to evaluate whether *IPPQ* could change the presynaptic levels of CaV2.2. We found that *IPPQ* decreased CaV2.2 presynaptic levels (Figs. 8B and C). Notably, *IPPQ* did not affect the localization of the NaV1.7 voltage-gated sodium channel NaV1.7 (Figs. 8B and C). These results demonstrate that interfering with the CaV2.2 AID/beta subunit interaction specifically reduces the presynaptic localization of the CaV2.2 in vivo.

3.6. Inhibition of spinal calcitonin gene–related peptide release by *IPPQ*

CaV2.2 activity controls C-fiber sEPSCs and the release of the nociceptive neurotransmitter CGRP. Because *IPPQ* inhibited CaV2.2 and sEPSC frequency, we hypothesized that evoked spinal CGRP release would be inhibited by *IPPQ*. To test this, we measured CGRP release evoked by depolarization (90-mM KCl, a concentration that activates low- and high-voltage-activated Ca^{2+} channels[84]) in an ex vivo preparation of the lumbar region of rat spinal cord. Enzyme-linked immunosorbent assay (ELISA) was used to measure CGRP content; samples were collected every 10 minutes. We chose 10 minutes because this incubation period was sufficient to cause a reduction in depolarization-triggered calcium influx in DRG neurons in vitro (Figs. 9A–C). Basal CGRP levels were ~8.2 $pg{\cdot}mL^{-1}{\cdot}mg^{-1}$ of tissue (Fig. 9D, fractions #1 & 2). Before stimulation, control (0.1% DMSO) or a 20-μM *IPPQ* was added for 10 minutes (Fig. 9D, fraction #3). Although *IPPQ* application did not elicit any CGRP release from the spinal cords (Fig. 9D, fraction #3), depolarization evoked CGRP release from spinal cord, which was inhibited by ~63% by compound *IPPQ* (Fig. 9D, fraction #4). These results show that inhibiting CaV2.2 by targeting the CaVβ–CaVα interface with *IPPQ* results in decreased depolarization-evoked CGRP release.

3.7. Broad antinociceptive efficacy of *IPPQ*

The peptide ω-conotoxin GVIA remains a defining ligand for CaV2.2 and is marketed as Prialt (Primary Alternative to Morphine) for relief of chronic and cancer-related pain,[67] establishing the therapeutic value of targeting CaV2.2. *IPPQ* increased withdrawal latency to a heat stimulus in naive rats (Fig. 10A), demonstrating antinociceptive potential. Furthermore, CaV2.2 is known to be involved in postsurgical pain,[26] neuropathic pain,[91] chemotherapy-induced neuropathy,[37] HIV-induced sensory neuropathy,[57] and neurofibromatosis type 1 (NF1)-related pain.[60] Thus, we performed an analgesic appraisal of *IPPQ* on heat and tactile sensitivity of rats in vivo. We chose to administer *IPPQ* intrathecally (2 μg in 5 μL) to directly reach the site of action of CaV2.2 in the dorsal horn, the presynaptic termini of pain fibers that synapse with spinal cord neurons and require CaV2.2 for the release of neurotransmitter at these synapses. *IPPQ* reversed mechanical allodynia and thermal hyperalgesia in models of NF1-related pain (Fig. 10B), postsurgical pain (Figs. 10C–D), and neuropathic pain (Figs. 10E–F). *IPPQ* was also efficient in reversing mechanical allodynia in paclitaxel-induced peripheral neuropathy (Fig. 10G) and HIV-induced sensory neuropathy (Fig. 10H). The reversal lasted about 2 to 3 hours across the behavioral paradigms tested, consistent with a plasma half-life of 2.2 hours for *IPPQ* (data not shown). These results demonstrate the utility of *IPPQ* to modulate painful sensations in rodents.

3.8. *IPPQ* does not cause motor impairment

The clinically used CaV2.2 drug Prialt (ziconotide) produces akinesia when injected into the brain.[48] To test whether *IPPQ* would elicit a similarly undesirable effect, we used the rotarod test to assess rats' motor function after an i.c.v. injection of *IPPQ* (2 μg in 5 μL). Rats were followed for 90 minutes after the injection, and no motor impairment was observed (supplementary Fig. 2, available at http://links.lww.com/PAIN/A760) after *IPPQ*

brain injection. We did not observe other behavioral alterations such as seizures in any of the animals tested.

3.9. *IPPQ* works through a spinal mechanism and does not affect anxiety

IPPQ was tested in acute thermal pain models (hot-plate or tail-flick) because CaV2.2 blockers have been reported to be more effective against chronic than acute pain.[47] The tail-flick test is considered predominantly spinal because it can be observed even in animals with spinal cord transection that have severed descending pathways[20] or animals under anesthesia, which is not the case for the paw lifting/jumping, twitching, and licking behavior observed in the hot-plate test. When a dose (15 mg/kg) of *IPPQ* was intraperitoneally administered in acute thermal pain models, the latency times were not affected in the hot-plate test (predominantly supraspinal) but increased in the tail-flick test (predominantly spinal) (Figs. 11A and B). Gabapentin administration (100 mg/kg) was used a control for the hot-plate and tail-flick tests: it increased paw withdrawal latencies in the hot-plate test but was without effect at this dose on tail-flick latencies (Figs. 11C and D), consistent with what has been reported previously.[5] The lack of effect *IPPQ* administered intraperitoneally in the hot-plate compared with tail-flick points to a specific action of *IPPQ* on processes implicated in the tail-flick test, similarly to what has been observed in the $\alpha 1B^{-/-}$ knockout mice[69] or with specific blockers of CaV2.2.[5]

As it has been previously demonstrated that inhibition of CaV2.2-mediated signaling induces alterations in the neuronal network involved in anxiety-related behaviors,[42,93] we next tested the effects of *IPPQ* on anxiety using the elevated plus maze test. Time spent in the open arms of the elevated plus maze, time spent in the closed arms, and number of entries in the open arms did not differ between animal treated with *IPPQ* or its vehicle (Figs. 11E and F), suggesting that *IPPQ* does not affect anxiety-related behaviors.

4. Discussion

The present work used a rational structure-based design strategy to identify a new class of nonopioid, analgesic compounds targeting the CaVα–CaVβ interface. The quinazoline analog *IPPQ* (1) specifically bound to CaVβ, (2) inhibited the biochemical interaction between CaVβ2 and the AID of CaV2.2 and to a lesser extent between CaVβ2 and the AID of CaV2.1, but not other subtypes, (3) and functionally inhibited CaV2.2 function (acutely and chronically) across subtypes of DRG sensory neurons. *IPPQ* inhibited the presynaptic localization of CaV2.2 in vivo as well as inhibiting spinal neurotransmission, which resulted in decreased neurotransmitter release from the spinal cord. Finally, *IPPQ* was antinociceptive in naive rats and reversed mechanical allodynia and thermal hyperalgesia in rodent models of acute (postsurgical), neuropathic (spared nerve ligation, paclitaxel, or HIV-induced sensory neuropathy), and genetic (NF1-related) pain. No adverse effects were observed for *IPPQ* in rats or mice. These results are an instructive example that pharmacological disruption of the CaVα–CaVβ interface can result in a selective, safe, and broadly antinociceptive compound, setting the stage for structure–activity relationship studies to improve on this lead molecule for the development of novel pain therapeutics.

The CaVα–CaVβ interaction shapes activity and trafficking of all subtypes of high-voltage-gated calcium channels (ie, L-, N-, P/Q-, and R-type). Before the crystallization of CaVβ subunits, Wyeth-Ayerst Research used a high-throughput yeast 2-hybrid screen to identity compounds that disrupt α1b and β3 and found WAY141520, which inhibited calcium currents with an IC_{50} of 95 μM, with some inhibitory activity against CaV2.2 but was not tested against other channels nor was its mechanism of action studied.[92] Structural studies of CaVβs in early 2000s[16,63,79] with a fragment of the α subunit revealed a high homology between the various α–β subunits, predicting that targeting of this interface would result in nonselective compounds. The details of this interface have been extensively studied in deep thermodynamic detail for all of the CaV1 and CaV2 AIDs and that has defined the hotspots on both sides of this interaction.[80] Of the 3 "hot spots" identified by the Minor laboratory, V241 makes no contacts with the AID, N390 does not contribute to the energetics of the interaction, and only I343 is important, interacting with one of the core residues that comprise the AID hotspot (CaV1.2 Y437).[80] Despite these theoretical predictions, *IPPQ* exhibited selectivity for CaV2.2. *IPPQ* interacts with CaVα–CaVβ domain mainly at the lipophilic pocket defined by Val 339–Ile 343.[79] The AID sequence aligns (side chains of critical residues Y437, W440, and I441; Fig. 1C) with the quinazoline ring and phenylpropyl group of *IPPQ*. We hypothesize that these interactions result in high selectivity for *IPPQ*. That *IPPQ* reduced the binding affinity between CaVβ and AID peptides of CaV2.2 (by ~17.3-fold) and CaV2.1 (by ~5-fold) but had no effect on binding to other channel subtypes demonstrates selectivity for the interaction. Although this selectivity was unexpected, the electrophysiology recordings on sensory neurons confirmed a selectivity for CaV2.2 while the electrophysiology recordings in heterologous cells, performed in an independent laboratory, confirmed inhibition through CaV2.2 and CaVβ1b, CaVβ2a, and CaVβ3, irrespective of the presence of the α2δ−1 subunit. Inhibiting CaV2.2 with *IPPQ* did not show the typical regulation of the channel's gating property by CaVβs.[12] But this is consistent with a previous report that demonstrated no effect on voltage-dependent activation of high-voltage-activated calcium channels upon deletion of CaVβ3 subunit in DRGs.[43] It has also been reported that the orientation of CaVβ relative to the α subunit of CaV2.2 subunit is critical for its regulation of channel activity with insertions or deletions of the AID linker, which are expected to maintain the α-helical structure of the linker but induce a rotation of CaVβ with respect to CaVα1, diminishing CaVβ regulation of activation and inactivation.[82] Thus, *IPPQ* could possibly induce conformational changes that result in disrupt the rigidity of the α-helix, which may in turn explain the lack of effects on biophysical properties.

Presynaptic voltage-dependent calcium channels, controlling calcium influx, serve as the trigger for release of glutamate from the terminals of the primary afferent fibers onto spinal dorsal horn neurons.[45] The interruption of CaVα–CaVβ interaction by *IPPQ* might result in the inhibition of excitatory synaptic inputs to SG neurons. The decrease of sEPSC frequency suggested that *IPPQ* inhibited the glutamatergic excitatory inputs by a presynaptic mechanism. It is generally accepted that the changes in frequency of mEPSCs reflects an alteration of presynaptic neurotransmitter release probability, and that the changes in mEPSC amplitude indicate less neurotransmitter content per quanta (per presynaptic vesicle), fewer postsynaptic receptors, or a change in the type of receptors at postsynaptic

sites (ie, a change in the single channel conductance of receptors).[32] *IPPQ* also inhibited both frequency and amplitude of mEPSCs. This is consistent with a previous report that specific antagonists for one or more high-threshold-activated Ca^{2+} channels suppress release of transmitter by presynaptic impulses at central synapses, thereby also reducing the postsynaptic response.[6] Moreover, the PPR protocol, used to investigate the short-term plasticity characteristics of synapse, is a widely accepted approach for assessing the synaptic sites of action.[77] The increase of PPR induced by paired-pulse stimulation further implicates a presynaptic origin for the mechanism of *IPPQ*'s action on spinal synaptic neurotransmission. In support of this, we observed decreased levels of spinal presynaptic CaV2.2 after *IPPQ* treatment, thus reinforcing the assertion that *IPPQ* acts presynaptically.

That *IPPQ* was effective and safe in vivo likely stems from the restricted expression patterns of the CaVβ subunits. For example, CaVβ1 is expressed in skeletal muscle,[31] CaVβ2 is expressed in the heart and at very low levels in the central nervous system (CNS),[44] CaVβ3 expression is found in smooth muscle and in the CNS (including the spinal cord),[44] and CaVβ4 is expressed predominantly in the cerebellum.[44] CaV2.2 is expressed in the brain and in the sensory neurons.[14] Thus, only in the brain and sensory neurons does CaV2.2 expression overlap with that of CaVβ3 and CaVβ4. Our in vitro results demonstrated that only coexpression of the CaVβ3/4 subunits with CaV2.2 resulted in high Ca^{2+} currents while CaVβ1/2 coexpression with CaV2.2 (a configuration that is not physiologically relevant because these subunits are primarily expressed in skeletal or heart muscles) resulted in low Ca^{2+} currents. *IPPQ* inhibited Ca^{2+} currents when coexpressed with CaVβ1/2/3, but not CaVβ4. Thus in vivo, *IPPQ* would only target CaVβ3–CaV2.2 coupling because of the overlapping tissue distribution of these subunits. The notion that CaV2.2 functions with CaVβ3 to mediate nociception in vivo is supported by mouse models lacking either CaV2.2[69] or CaVβ3[61] with these transgenic mice demonstrating resistance to pain sensation. Notably, CaVβ3 expression is increased in neuropathic pain,[43] in parallel with increased voltage-gated calcium channel function. Thus, the specific uncoupling of CaVβ3–CaV2.2, but not CaVβ4–CaV2.2, may underpin the calcium channel subtype selectivity of *IPPQ* and its in vivo efficacy for the reversal of chronic pain behaviors.

A common denominator in the neuropathic models appraised here is the plasticity of CaV2.2: targeted truncation of neurofibromin, achieved by acute CRISPR/Cas9 editing of the *Nf1* gene in adult rats, and resulted in increases of CaV2.2 currents[60]; spinal nerve ligation increased CaV2.2 expression in the synaptic plasma membranes of the dorsal horn[41]; and the *Cacna1b* gene encoding CaV2.2 is highly upregulated in a rodent model of HIVSNL treated with gp120 compared with sham-treated controls.[46] Previous reports have shown attenuation of allodynia by a CaV2.2-blocking compound in the paw incision model of surgical pain[26] and the paclitaxel-induced model of chemotherapy-induced peripheral neuropathy.[8] The broad antinociceptive potential of *IPPQ* across acute and neuropathic models, in 2 species, can be attributed to its biochemical and functional inhibition of the CaVα–CaVβ interaction, a mechanism distinct from direct block of CaV2.2 by small molecules covering various pharmacophores.[90]

Therapeutic management strategies for chronic pain usually involve the use of opioid molecules. These compounds primarily act on the MOR expressed on DRG sensory neurons

to provide analgesia. CaV2.2 can be inhibited downstream of G(i/o)-type G protein–coupled receptor signaling as shown upon morphine to the MOR or the α-conotoxin Vc1.1 binding to be GABA-B receptor.[33,53,54] In neuropathic pain, alternative splicing of CaV2.2 mRNA leads to 2 different CaV2.2 isoforms containing either the exon 37a (e37a) or e37b in sensory neurons.[7] After a neuropathic injury, expression of e37a is lost, resulting in an enrichment of e37b containing CaV2.2 in sensory neurons.[2] This switch in alternative splicing is an important event underlying resistance and tolerance to opioids since the remaining e37b containing CaV2.2 is resistant to the inhibition mediated by opioids.[3] No alternative splicing has been reported in the binding region between CaVα and CaVβ. Thus, targeting this interface using *IPPQ* is unlikely to be susceptible to similar tolerance mechanisms in neuropathic pain.

Although the CaV2.2-inhibiting drug ziconotide (Prialt) is effective in chronic and cancer-related pain,[67] it requires intrathecal dosing to circumvent systemic side effects that include confusion, depression, hallucinations, decreased alertness, somnolence, orthostatic hypotension, and nausea.[71] These are due to the direct blocking of CaV2.2 in the brain. Notably, when Prialt was injected i.c.v. in mice, it induced akinesia that would also decrease rotarod performance.[48] We observed no effect on rotarod performance in *IPPQ*-injected rats. If the rats had experienced akinesia, decreased alertness, or orthostatic hypotension, their rotarod performance would have been impaired accordingly. Thus, *IPPQ* treatment did not induce any of the side effect related to direct CaV2.2 inhibition throughout the brain and exhibits a better safety profile compared with the FDA-approved drug Prialt. Thus, a small molecule, such as *IPPQ*, devoid of these encumbrances and lacking a nonopioid mechanism would be a welcome addition to the armamentarium of the pain physician for managing chronic pain.

Supplementary Material

Refer to Web version on PubMed Central for supplementary material.

Acknowledgements

This work was supported by a Career Development Award from the Arizona Health Science Center to M. Khanna, grants from the National Natural Science Foundation of China (81603088) and National Key Project of Research and Development of China (2018YFC1705501) to J. Yu, National Institutes of Health awards (NINDS K08 to A.M. Patwardhan; R01NS098772 from the National Institute of Neurological Disorders and Stroke and R01DA042852 from the National Institute on Drug Abuse to R. Khanna); and a Neurofibromatosis New Investigator Award from the Department of Defense Congressionally Directed Military Medical Research and Development Program (NF1000099) to R. Khanna.

References

[1]. Adams DJ, Callaghan B, Berecki G. Analgesic conotoxins: block and G protein-coupled receptor modulation of N-type (Ca(V) 2.2) calcium channels. Br J Pharmacol 2012;166:486–500. [PubMed: 22091786]

[2]. Altier C, Dale CS, Kisilevsky AE, Chapman K, Castiglioni AJ, Matthews EA, Evans RM, Dickenson AH, Lipscombe D, Vergnolle N, Zamponi GW. Differential role of N-type calcium channel splice isoforms in pain. J Neurosci 2007;27:6363–73. [PubMed: 17567797]

[3]. Andrade A, Denome S, Jiang YQ, Marangoudakis S, Lipscombe D. Opioid inhibition of N-type Ca2+ channels and spinal analgesia couple to alternative splicing. Nat Neurosci 2010;13:1249–56. [PubMed: 20852623]

[4]. Augustine GJ, Charlton MP, Smith SJ. Calcium entry and transmitter release at voltage-clamped nerve terminals of squid. J Physiol 1985;367: 163–81. [PubMed: 2865362]

[5]. Aydin ON, Ek RO, Temoçin S, Uğur B, Alaçam B, Şen S. The antinociceptive effects of systemic administration of tramadol, gabapentin and their combination on mice model of acute pain. Agri 2012;24:49–55. [PubMed: 22865488]

[6]. Bao J, Li JJ, Perl ER. Differences in Ca2+ channels governing generation of miniature and evoked excitatory synaptic currents in spinal laminae I and II. J Neurosci 1998;18:8740–50. [PubMed: 9786981]

[7]. Bell TJ, Thaler C, Castiglioni AJ, Helton TD, Lipscombe D. Cell-specific alternative splicing increases calcium channel current density in the pain pathway. Neuron 2004;41:127–38. [PubMed: 14715140]

[8]. Bellampalli SS, Ji Y, Moutal A, Cai S, Wijeratne EMK, Gandini MA, Yu J, Chefdeville A, Dorame A, Chew LA, Madura CL, Luo S, Molnar G, Khanna M, Streicher JM, Zamponi GW, Gunatilaka AAL, Khanna R. Betulinic acid, derived from the desert lavender hyptis emoryi, attenuates paclitaxel-, HIV-, and nerve injury-associated peripheral sensory neuropathy via block of N- and T-type calcium channels. PAIN 2019;160:117–35. [PubMed: 30169422]

[9]. Bourinet E, Zamponi GW. Voltage gated calcium channels as targets for analgesics. Curr Top Med Chem 2005;5:539–46. [PubMed: 16022676]

[10]. Brennan TJ, Vandermeulen EP, Gebhart GF. Characterization of a rat model of incisional pain. PAIN 1996;64:493–501. [PubMed: 8783314]

[11]. Brittain JM, Duarte DB, Wilson SM, Zhu W, Ballard C, Johnson PL, Liu N, Xiong W, Ripsch MS, Wang Y, Fehrenbacher JC, Fitz SD, Khanna M, Park CK, Schmutzler BS, Cheon BM, Due MR, Brustovetsky T, Ashpole NM, Hudmon A, Meroueh SO, Hingtgen CM, Brustovetsky N, Ji RR, Hurley JH, Jin X, Shekhar A, Xu XM, Oxford GS, Vasko MR, White FA, Khanna R. Suppression of inflammatory and neuropathic pain by uncoupling CRMP-2 from the presynaptic Ca(2)(+) channel complex. Nat Med 2011;17: 822–9. [PubMed: 21642979]

[12]. Buraei Z, Yang J. Structure and function of the beta subunit of voltage-gated Ca(2)(+) channels. Biochim Biophys Acta 2013;1828:1530–40. [PubMed: 22981275]

[13]. Cao YQ. Voltage-gated calcium channels and pain. PAIN 2006;126:5–9. [PubMed: 17084979]

[14]. Castiglioni AJ, Raingo J, Lipscombe D. Alternative splicing in the C-terminus of CaV2.2 controls expression and gating of N-type calcium channels. J Physiol 2006;576:119–34. [PubMed: 16857708]

[15]. Chaplan SR, Bach FW, Pogrel JW, Chung JM, Yaksh TL. Quantitative assessment of tactile allodynia in the rat paw. J Neurosci Methods 1994; 53:55–63. [PubMed: 7990513]

[16]. Chen YH, Li MH, Zhang Y, He LL, Yamada Y, Fitzmaurice A, Shen Y, Zhang H, Tong L, Yang J. Structural basis of the alpha1-beta subunit interaction of voltage-gated Ca2+ channels. Nature 2004;429:675–80. [PubMed: 15170217]

[17]. Choe W, Messinger RB, Leach E, Eckle VS, Obradovic A, Salajegheh R, Jevtovic-Todorovic V, Todorovic SM. TTA-P2 is a potent and selective blocker of T-type calcium channels in rat sensory neurons and a novel antinociceptive agent. Mol Pharmacol 2011;80:900–10. [PubMed: 21821734]

[18]. Cizkova D, Marsala J, Lukacova N, Marsala M, Jergova S, Orendacova J, Yaksh TL. Localization of N-type Ca2+ channels in the rat spinal cord following chronic constrictive nerve injury. Expbrain Res 2002;147: 456–63.

[19]. Coan KE, Shoichet BK. Stoichiometry and physical chemistry of promiscuous aggregate-based inhibitors. J Am Chem Soc 2008;130: 9606–12. [PubMed: 18588298]

[20]. Dávidová A, Schreiberová A, Kolesaŕ D, Capková L, Krizanová O, Lukácová N. Spinal cord transection significantly influences nNOS-IR in neuronal circuitry that underlies the tail-flick reflex activity. Cell Mol Neurobiol 2009;29:879–86. [PubMed: 19291395]

[21]. Dixon WJ. Efficient analysis of experimental observations. Annu Rev Pharmacol Toxicol 1980;20:441–62. [PubMed: 7387124]

[22]. Dolphin AC. Calcium channel diversity: multiple roles of calcium channel subunits. Curr Opin Neurobiol 2009;19:237–44. [PubMed: 19559597]

[23]. Feldman P, Khanna R. Challenging the catechism of therapeutics for chronic neuropathic pain: targeting CaV2.2 interactions with CRMP2 peptides. Neurosci Lett 2013;557:27–36. [PubMed: 23831344]

[24]. Feng ZP, Hamid J, Doering C, Bosey GM, Snutch TP, Zamponi GW. Residue Gly1326 of the N-type calcium channel alpha 1B subunit controls reversibility of omega-conotoxin GVIA and MVIIA block. J Biol Chem 2001;276:15728–35. [PubMed: 11279062]

[25]. Finnerup NB, Otto M, McQuay HJ, Jensen TS, Sindrup SH. Algorithm for neuropathic pain treatment: an evidence based proposal. PAIN 2005; 118:289–305. [PubMed: 16213659]

[26]. Francois-Moutal L, Wang Y, Moutal A, Cottier KE, Melemedjian OK, Yang X, Wang Y, Ju W, Largent-Milnes TM, Khanna M, Vanderah TW, Khanna R. A membrane-delimited N-myristoylated CRMP2 peptide aptamer inhibits CaV2.2 trafficking and reverses inflammatory and postoperative pain behaviors. PAIN 2015;156:1247–64. [PubMed: 25782368]

[27]. Friesner RA, Murphy RB, Repasky MP, Frye LL, Greenwood JR, Halgren TA, Sanschagrin PC, Mainz DT. Extra precision glide: docking and scoring incorporating a model of hydrophobic enclosure for protein-ligand complexes. J Med Chem 2006;49:6177–96. [PubMed: 17034125]

[28]. Hargreaves K, Dubner R, Brown F, Flores C, Joris J. A new and sensitive method for measuring thermal nociception in cutaneous hyperalgesia. PAIN 1988;32:77–88. [PubMed: 3340425]

[29]. Heckl D, Kowalczyk MS, Yudovich D, Belizaire R, Puram RV, McConkey ME, Thielke A, Aster JC, Regev A, Ebert BL. Generation of mouse models of myeloid malignancy with combinatorial genetic lesions using CRISPRCas9 genome editing. Nat Biotechnol 2014;32:941–6. [PubMed: 24952903]

[30]. Heinke B, Balzer E, Sandkuhler J. Pre- and postsynaptic contributions of voltage-dependent Ca2+ channels to nociceptive transmission in rat spinal lamina I neurons. Eur J Neurosci 2004;19:103–11. [PubMed: 14750968]

[31]. Hofmann F, Biel M, Flockerzi V. Molecular basis for Ca2+ channel diversity. Annu Rev Neurosci 1994;17:399–418. [PubMed: 8210181]

[32]. Huang H, Trussell LO. Presynaptic HCN channels regulate vesicular glutamate transport. Neuron 2014;84:340–6. [PubMed: 25263752]

[33]. Huynh TG, Cuny H, Slesinger PA, Adams DJ. Novel mechanism of voltage-gated N-type (Cav2.2) calcium channel inhibition revealed through alpha-conotoxin Vc1.1 activation of the GABA(B) receptor. Mol Pharmacol 2015;87:240–50. [PubMed: 25425625]

[34]. Ikeda SR. Voltage-dependent modulation of N-type calcium channels by G-protein beta gamma subunits. Nature 1996;380:255–8. [PubMed: 8637575]

[35]. Irwin JJ, Duan D, Torosyan H, Doak AK, Ziebart KT, Sterling T, Tumanian G, Shoichet BK. An aggregation advisor for ligand discovery. J Med Chem 2015;58:7076–87. [PubMed: 26295373]

[36]. Jiang YQ, Andrade A, Lipscombe D. Spinal morphine but not ziconotide or gabapentin analgesia is affected by alternative splicing of voltage-gated calcium channel CaV2.2 pre-mRNA. Mol Pain 2013;9:67. [PubMed: 24369063]

[37]. Kawakami K, Chiba T, Katagiri N, Saduka M, Abe K, Utsunomiya I, Hama T, Taguchi K. Paclitaxel increases high voltage-dependent calcium channel current in dorsal root ganglion neurons of the rat. J Pharmacol Sci 2012;120:187–95. [PubMed: 23090716]

[38]. Khanna R, Li Q, Bewersdorf J, Stanley EF. The presynaptic CaV2.2 channel-transmitter release site core complex. Eur J Neurosci 2007;26: 547–59. [PubMed: 17686036]

[39]. Kim C, Jeon D, Kim YH, Lee CJ, Kim H, Shin HS. Deletion of N-type Ca2+ channel Cav2.2 results in hyperaggressive behaviors in mice. J Biol Chem 2009;284:2738–45. [PubMed: 19004821]

[40]. Kim C, Jun K, Lee T, Kim SS, McEnery MW, Chin H, Kim HL, Park JM, Kim DK, Jung SJ, Kim J, Shin HS. Altered nociceptive response in mice deficient in the alpha(1B) subunit of the voltage-dependent calcium channel. Mol Cell Neurosci 2001;18:235–45. [PubMed: 11520183]

[41]. Lai CY, Ho YC, Hsieh MC, Wang HH, Cheng JK, Chau YP, Peng HY. Spinal fbxo3-dependent Fbxl2 ubiquitination of active zone protein RIM1alpha mediates neuropathic allodynia through CaV2.2 activation. J Neurosci 2016;36:9722–38. [PubMed: 27629721]

[42]. Lee MS. Recent progress in the discovery and development of N-type calcium channel modulators for the treatment of pain. Prog Med Chem 2014;53:147–86. [PubMed: 24418610]

[43]. Li L, Cao XH, Chen SR, Han HD, Lopez-Berestein G, Sood AK, Pan HL. Up-regulation of Cavbeta3 subunit in primary sensory neurons increases voltage-activated Ca2+ channel activity and nociceptive input in neuropathic pain. J Biol Chem 2012;287:6002–13. [PubMed: 22187436]

[44]. Ludwig A, Flockerzi V, Hofmann F. Regional expression and cellular localization of the alpha1 and beta subunit of high voltage-activated calcium channels in rat brain. J Neurosci 1997;17:1339–49. [PubMed: 9006977]

[45]. Luebke JI, Dunlap K, Turner TJ. Multiple calcium channel types control glutamatergic synaptic transmission in the hippocampus. Neuron 1993; 11:895–902. [PubMed: 7902110]

[46]. Maratou K, Wallace VC, Hasnie FS, Okuse K, Hosseini R, Jina N, Blackbeard J, Pheby T, Orengo C, Dickenson AH, McMahon SB, Rice AS. Comparison of dorsal root ganglion gene expression in rat models of traumatic and HIV-associated neuropathic pain. Eur J Pain 2009;13: 387–98. [PubMed: 18606552]

[47]. McGivern JG. Ziconotide: a review of its pharmacology and use in the treatment of pain. Neuropsychiatr Dis Treat 2007;3:69–85. [PubMed: 19300539]

[48]. McIntosh JM, Corpuz GO, Layer RT, Garrett JE, Wagstaff JD, Bulaj G, Vyazovkina A, Yoshikami D, Cruz LJ, Olivera BM. Isolation and characterization of a novel conus peptide with apparent antinociceptive activity. J Biol Chem 2000;275:32391–7. [PubMed: 10900201]

[49]. Meyer B, Klein J, Mayer M, Meinecke R, Möller H, Neffe A, Schuster O, Wülfken J, Ding Y, Knaie O, Labbe J, Palcic MM, Hindsgaul O, Wagner B, Ernst B. Saturation transfer difference NMR spectroscopy for identifying ligand epitopes and binding specificities. Ernst Schering Res Found Workshop 2004;44:149–67.

[50]. Meyer B, Peters T. NMR spectroscopy techniques for screening and identifying ligand binding to protein receptors. Angew Chem Int Ed Engl 2003;42:864–90. [PubMed: 12596167]

[51]. Milligan ED, O'Connor KA, Nguyen KT, Armstrong CB, Twining C, Gaykema RP, Holguin A, Martin D, Maier SF, Watkins LR. Intrathecal HIV-1 envelope glycoprotein gp120 induces enhanced pain states mediated by spinal cord proinflammatory cytokines. J Neurosci 2001;21:2808–19. [PubMed: 11306633]

[52]. Mintz IM, Venema VJ, Swiderek KM, Lee TD, Bean BP, Adams ME. P-type calcium channels blocked by the spider toxin omega-Aga-IVA. Nature 1992;355:827–9. [PubMed: 1311418]

[53]. Moises HC, Rusin KI, Macdonald RL. Mu- and kappa-opioid receptors selectively reduce the same transient components of high-threshold calcium current in rat dorsal root ganglion sensory neurons. J Neurosci 1994;14:5903–16. [PubMed: 7931552]

[54]. Moises HC, Rusin KI, Macdonald RL. mu-opioid receptor-mediated reduction of neuronal calcium current occurs via a G(o)-type GTP-binding protein. J Neurosci 1994;14:3842–51. [PubMed: 8207492]

[55]. Moutal A, Cai S, Luo S, Voisin R, Khanna R. CRMP2 is necessary for Neurofibromatosis type 1 related pain. Channels (Austin) 2018;12:47–50. [PubMed: 28837387]

[56]. Moutal A, Chew LA, Yang X, Wang Y, Yeon SK, Telemi E, Meroueh S, Park KD, Shrinivasan R, Gilbraith KB, Qu C, Xie JY, Patwardhan A, Vanderah TW, Khanna M, Porreca F, Khanna R. (S)-lacosamide inhibition of CRMP2 phosphorylation reduces postoperative and neuropathic pain behaviors through distinct classes of sensory neurons identified by constellation pharmacology. PAIN 2016;157:1448–63. [PubMed: 26967696]

[57]. Moutal A, Li W, Wang Y, Ju W, Luo S, Cai S, François-Moutal L, Perez-Miller S, Hu J, Dustrude ET, Vanderah TW, Gokhale V, Khanna M, Khanna R. Homology-guided mutational analysis reveals the functional requirements for antinociceptive specificity of collapsin response mediator protein 2-derived peptides. Br J Pharmacol 2018;175:2244–60. [PubMed: 28161890]

[58]. Moutal A, Sun L, Yang X, Li W, Cai S, Luo S, Khanna R. CRMP2-Neurofibromin interface drives NF1-related pain. Neuroscience 2018; 381:79–90. [PubMed: 29655575]

[59]. Moutal A, Wang Y, Yang X, Ji Y, Luo S, Dorame A, Bellampalli SS, Chew LA, Cai S, Dustrude ET, Keener JE, Marty MT, Vanderah TW, Khanna R. Dissecting the role of the CRMP2-neurofibromin complex on pain behaviors. PAIN 2017;158:2203–21. [PubMed: 28767512]

[60]. Moutal A, Yang X, Li W, Gilbraith KB, Luo S, Cai S, Francois-Moutal L, Chew LA, Yeon SK, Bellampalli SS, Qu C, Xie JY, Ibrahim MM, Khanna M, Park KD, Porreca F, Khanna R. CRISPR/Cas9 editing of Nf1 gene identifies CRMP2 as a therapeutic target in neurofibromatosis type 1 (NF1)-related pain that is reversed by (S)-Lacosamide. PAIN 2017;158:2301–19. [PubMed: 28809766]

[61]. Murakami M, Nakagawasai O, Yanai K, Nunoki K, Tan-No K, Tadano T, Iijima T. Modified behavioral characteristics following ablation of the voltage-dependent calcium channel beta3 subunit. Brain Res 2007; 1160:102–12. [PubMed: 17588550]

[62]. Newcomb R, Szoke B, Palma A, Wang G, Chen X, Hopkins W, Cong R, Miller J, Urge L, Tarczy-Hornoch K, Loo JA, Dooley DJ, Nadasdi L, Tsien RW, Lemos J, Miljanich G. Selective peptide antagonist of the class E calcium channel from the venom of the tarantula hysterocrates gigas. Biochemistry 1998;37:15353–62. [PubMed: 9799496]

[63]. Opatowsky Y, Chen CC, Campbell KP, Hirsch JA. Structural analysis of the voltage-dependent calcium channel beta subunit functional core and its complex with the alpha 1 interaction domain. Neuron 2004;42: 387–99. [PubMed: 15134636]

[64]. Pacchioni AM, Vallone J, Worley PF, Kalivas PW. Neuronal pentraxins modulate cocaine-induced neuroadaptations. J Pharmacol Exp Ther 2009;328:183–92. [PubMed: 18840757]

[65]. Pexton T, Moeller-Bertram T, Schilling JM, Wallace MS. Targeting voltage-gated calcium channels for the treatment of neuropathic pain: a review of drug development. Expert Opin Investig Drugs 2011;20: 1277–84.

[66]. Polomano RC, Mannes AJ, Clark US, Bennett GJ. A painful peripheral neuropathy in the rat produced by the chemotherapeutic drug, paclitaxel. PAIN 2001;94:293–304. [PubMed: 11731066]

[67]. Rauck RL, Wallace MS, Leong MS, Minehart M, Webster LR, Charapata SG, Abraham JE, Buffington DE, Ellis D, Kartzinel R. A randomized, double-blind, placebo-controlled study of intrathecal ziconotide in adults with severe chronic pain. J Pain Symptom Manage 2006;31:393–406. [PubMed: 16716870]

[68]. Richards MW, Butcher AJ, Dolphin AC. Ca2+ channel beta-subunits: structural insights AID our understanding. Trends Pharmacolsci 2004;25: 626–32.

[69]. Saegusa H, Kurihara T, Zong S, Kazuno A, Matsuda Y, Nonaka T, Han W, Toriyama H, Tanabe T. Suppression of inflammatory and neuropathic pain symptoms in mice lacking the N-type Ca2+ channel. EMBO J 2001; 20:2349–56. [PubMed: 11350923]

[70]. Sakaba T, Neher E. Quantitative relationship between transmitter release and calcium current at the calyx of held synapse. J Neurosci 2001;21: 462–76. [PubMed: 11160426]

[71]. Schmidtko A, Lötsch J, Freynhagen R, Geisslinger G. Ziconotide for treatment of severe chronic pain. Lancet 2010;375:1569–77. [PubMed: 20413151]

[72]. Scott DA, Wright CE, Angus JA. Actions of intrathecal omega-conotoxins CVID, GVIA, MVIIA, and morphine in acute and neuropathic pain in the rat. Eur J Pharmacol 2002;451:279–86. [PubMed: 12242089]

[73]. Smith MT, Cabot PJ, Ross FB, Robertson AD, Lewis RJ. The novel N-type calcium channel blocker, AM336, produces potent dose-dependent antinociception after intrathecal dosing in rats and inhibits substance P release in rat spinal cord slices. PAIN 2002;96:119–27. [PubMed: 11932068]

[74]. Stefanucci A, Lei W, Hruby VJ, Macedonio G, Luisi G, Carradori S, Streicher JM, Mollica A. Fluorescent-labeled bioconjugates of the opioid peptides biphalin and DPDPE incorporating fluorescein-maleimide linkers. Future Med Chem 2017;9:859–69. [PubMed: 28635314]

[75]. Teichert RW, Memon T, Aman JW, Olivera BM. Using constellation pharmacology to define comprehensively a somatosensory neuronal subclass. Proc Natl Acad Sci USA 2014;111:2319–24. [PubMed: 24469798]

[76]. Teichert RW, Raghuraman S, Memon T, Cox JL, Foulkes T, Rivier JE, Olivera BM. Characterization of two neuronal subclasses through constellation pharmacology. Proc Natl Acad Sci USA 2012;109: 12758–63. [PubMed: 22778416]

[77]. Tomoyose O, Kodama D, Ono H, Tanabe M. Presynaptic inhibitory effects of fluvoxamine, a selective serotonin reuptake inhibitor, on nociceptive excitatory synaptic transmission in spinal

superficial dorsal horn neurons of adult mice. J Pharmacol Sci 2014;126:136–45. [PubMed: 25252797]

[78]. Tsien RW, Lipscombe D, Madison DV, Bley KR, Fox AP. Multiple types of neuronal calcium channels and their selective modulation. Trends Neurosci 1988;11:431–8. [PubMed: 2469160]

[79]. Van PF, Clark KA, Chatelain FC, Minor DL Jr. Structure of a complex between a voltage-gated calcium channel beta-subunit and an alpha-subunit domain. Nature 2004;429:671–5. [PubMed: 15141227]

[80]. Van PF, Duderstadt KE, Clark KA, Wang M, Minor DL Jr. Alanine-scanning mutagenesis defines a conserved energetic hotspot in the CaValpha1 AID-CaVbeta interaction site that is critical for channel modulation. Structure 2008;16:280–94. [PubMed: 18275819]

[81]. Vendel AC, Terry MD, Striegel AR, Iverson NM, Leuranguer V, Rithner CD, Lyons BA, Pickard GE, Tobet SA, Horne WA. Alternative splicing of the voltage-gated Ca2+ channel beta4 subunit creates a uniquely folded N-terminal protein binding domain with cell-specific expression in the cerebellar cortex. J Neurosci 2006;26:2635–44. [PubMed: 16525042]

[82]. Vitko I, Shcheglovitov A, Baumgart JP, Arias-Olguín II, Murbartián J, Arias JM, Perez-Reyes E. Orientation of the calcium channel beta relative to the alpha(1)2.2 subunit is critical for its regulation of channel activity. PLoS One 2008;3:e3560. [PubMed: 18958281]

[83]. Westenbroek RE, Hell JW, Warner C, Dubel SJ, Snutch TP, Catterall WA. Biochemical properties and subcellular distribution of an N-type calcium channel alpha 1 subunit. Neuron 1992;9:1099–115. [PubMed: 1334419]

[84]. Wheeler DG, Groth RD, Ma H, Barrett CF, Owen SF, Safa P, Tsien RW. Ca(V)1 and Ca(V)2 channels engage distinct modes of Ca(2+) signaling to control CREB-dependent gene expression. Cell 2012;149:1112–24. [PubMed: 22632974]

[85]. Wilson SM, Brittain JM, Piekarz AD, Ballard CJ, Ripsch MS, Cummins TR, Hurley JH, Khanna M, Hammes NM, Samuels BC, White FA, Khanna R. Further insights into the antinociceptive potential of a peptide disrupting the N-type calcium channel-CRMP-2 signaling complex. Channels (Austin) 2011;5:449–56. [PubMed: 21829088]

[86]. Wilson SM, Moutal A, Melemedjian OK, Wang Y, Ju W, François-Moutal L, Khanna M, Khanna R. The functionalized amino acid (S)-lacosamide subverts CRMP2-mediated tubulin polymerization to prevent constitutive and activity-dependent increase in neurite outgrowth. Front Cel Neurosci 2014;8:196.

[87]. Wilson SM, Schmutzler BS, Brittain JM, Dustrude ET, Ripsch MS, Pellman JJ, Yeum TS, Hurley JH, Hingtgen CM, White FA, Khanna R. Inhibition of transmitter release and attenuation of anti-retroviral-associated and tibial nerve injury-related painful peripheral neuropathy by novel synthetic Ca2+ channel peptides. J Biol Chem 2012;287: 35065–77. [PubMed: 22891239]

[88]. Xie JY, Chew LA, Yang X, Wang Y, Qu C, Wang Y, Federici LM, Fitz SD, Ripsch MS, Due MR, Moutal A, Khanna M, White FA, Vanderah TW, Johnson PL, Porreca F, Khanna R. Sustained relief of ongoing experimental neuropathic pain by a CRMP2 peptide aptamer with low abuse potential. PAIN 2016;157:2124–40. [PubMed: 27537210]

[89]. Yaksh TL, Rudy TA. Chronic catheterization of the spinal subarachnoid space. Physiol Behav 1976;17:1031–6. [PubMed: 14677603]

[90]. Yamamoto T, Takahara A. Recent updates of N-type calcium channel blockers with therapeutic potential for neuropathic pain and stroke. Curr Top Med Chem 2009;9:377–95. [PubMed: 19442208]

[91]. Yang J, Xie MX, Hu L, Wang XF, Mai JZ, Li YY, Wu N, Zhang C, Li J, Pang RP, Liu XG. Upregulation of N-type calcium channels in the soma of uninjured dorsal root ganglion neurons contributes to neuropathic pain by increasing neuronal excitability following peripheral nerve injury. Brain Behav Immun 2018;71:52–65. [PubMed: 29709527]

[92]. Young K, Lin S, Sun L, Lee E, Modi M, Hellings S, Husbands M, Ozenberger B, Franco R. Identification of a calcium channel modulator using a high throughput yeast two-hybrid screen. Nat Biotechnol 1998; 16:946–50. [PubMed: 9788351]

[93]. Zamponi GW. Targeting voltage-gated calcium channels in neurological and psychiatric diseases. Nat Rev Drug Discov 2016;15:19–34. [PubMed: 26542451]

[94]. Zamponi GW, Lewis RJ, Todorovic SM, Arneric SP, Snutch TP. Role of voltage-gated calcium channels in ascending pain pathways. Brain Res Rev 2009;60:84–9. [PubMed: 19162069]

[95]. Zamponi GW, Snutch TP. Decay of prepulse facilitation of N type calcium channels during G protein inhibition is consistent with binding of a single Gbeta subunit. Proc Natl Acad Sci U S A 1998;95:4035–9. [PubMed: 9520488]

[96]. Zhang SH, Yu J, Lou GD, Tang YY, Wang RR, Hou WW, Chen Z. Widespread pain sensitization after partial infraorbital nerve transection in MRL/MPJ mice. PAIN 2016;157:740–9. [PubMed: 26588696]

[97]. Zhang Y, Xiao X, Zhang XM, Zhao ZQ, Zhang YQ. Estrogen facilitates spinal cord synaptic transmission via membrane-bound estrogen receptors: implications for pain hypersensitivity. J Biol Chem 2012;287: 33268–81. [PubMed: 22869379]

[98]. Zucker RS, Regehr WG. Short-term synaptic plasticity. Annu Rev Physiol 2002;64:355–405. [PubMed: 11826273]

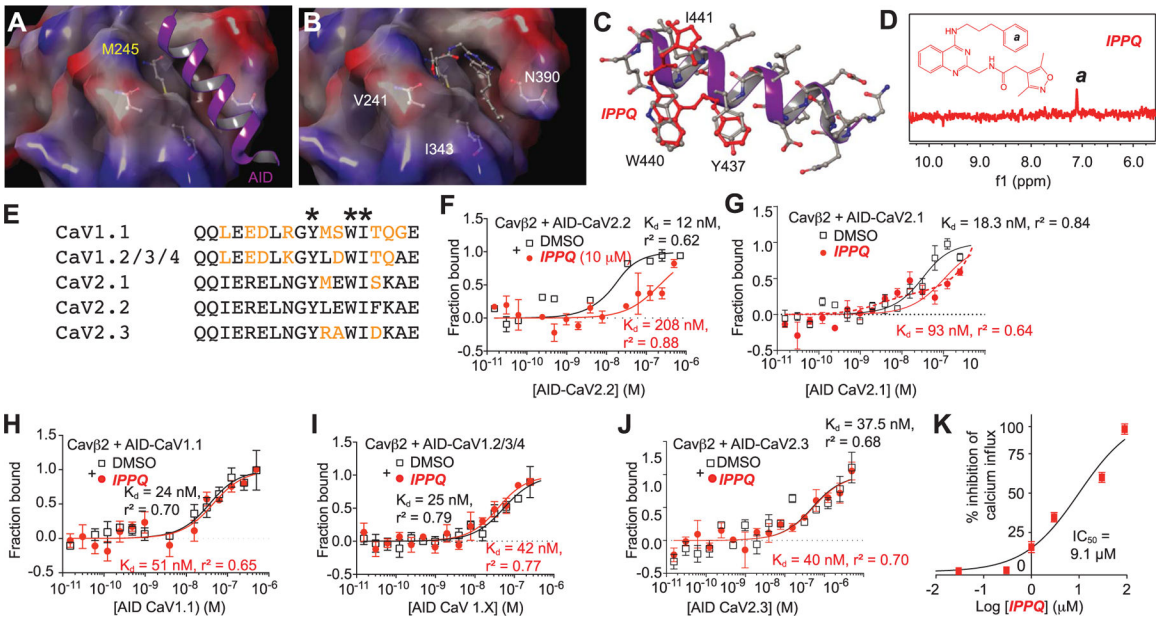

Figure 1.

Structure-guided high-throughput screen of CaVα–CaVβ interaction inhibitors identifies *IPPQ* (A) Space-filling model of the CaVβ2a subunit showing its α-binding pocket (ABP). A ribbon representation of the CaVα-interaction domain (AID, purple) and the AID's key interaction residue (M245) are highlighted. (B) Ball-and-stick representation of key ABP residues is shown (ie, V241, I343, and N390). (C) A 3-dimensional representation of *IPPQ* (red) overlaid on the AIDs reveals shared chemical features, especially at AID residues W440, I441, and Y437. (D) 1D ^{1}H STD NMR showing on-resonance difference spectrum for *IPPQ* (red); only regions that yielded a STD signal in the presence of *IPPQ* are plotted. The 2-dimensional chemical structure of compound *IPPQ* shows that region *a* corresponds with the STD signal highlighted. (E) Amino acid alignments of AID residues of the indicated calcium channel subtypes. Residues different from the CaV2.2 core AID sequence are denoted in orange. Asterisks denote the key residues conserved in all AID sequences involved in the interaction with the beta subunits. Microscale thermophoresis was used to determine dissociation constants for binding of AID-CaV2.2 (F), CaV2.1 (G), CaV1.1 (H), CaV1.2/3/4 (I) (500–0.01 nM), and CaV2.3 (J) to Beta2-CaVβ2-His (25 nM) in the presence (filled red circles) or absence of 10-μM *IPPQ* (open squares). Data are presented as mean ± SEM. The data were all fit with a one-site binding model, and the K_d and r^2 values are indicated. The data for Beta2-CaVβ2-His and AID-CaV2.1 in the presence of vehicle also fit well with a 2-site binding model (r^2 = 0.84) but yielded K_ds that were a 1000-fold higher than the one-binding site equation. In the presence of *IPPQ*, the data in panel (G) had a better fit (r^2 = 0.74) but yielded K_ds values of 2.3 nM (for the high affinity site) and ~81 mM (for the low-affinity site). (K) Concentration–response curve illustrates that *IPPQ* inhibits membrane depolarization-evoked Ca^{2+} influx in DRGs (n > 150 cells per concentration from 3 independent platings) in a concentration-dependent manner. *IPPQ* was applied overnight (15–18 hours). AID, alpha interaction domain; CaV, voltage-gated calcium.

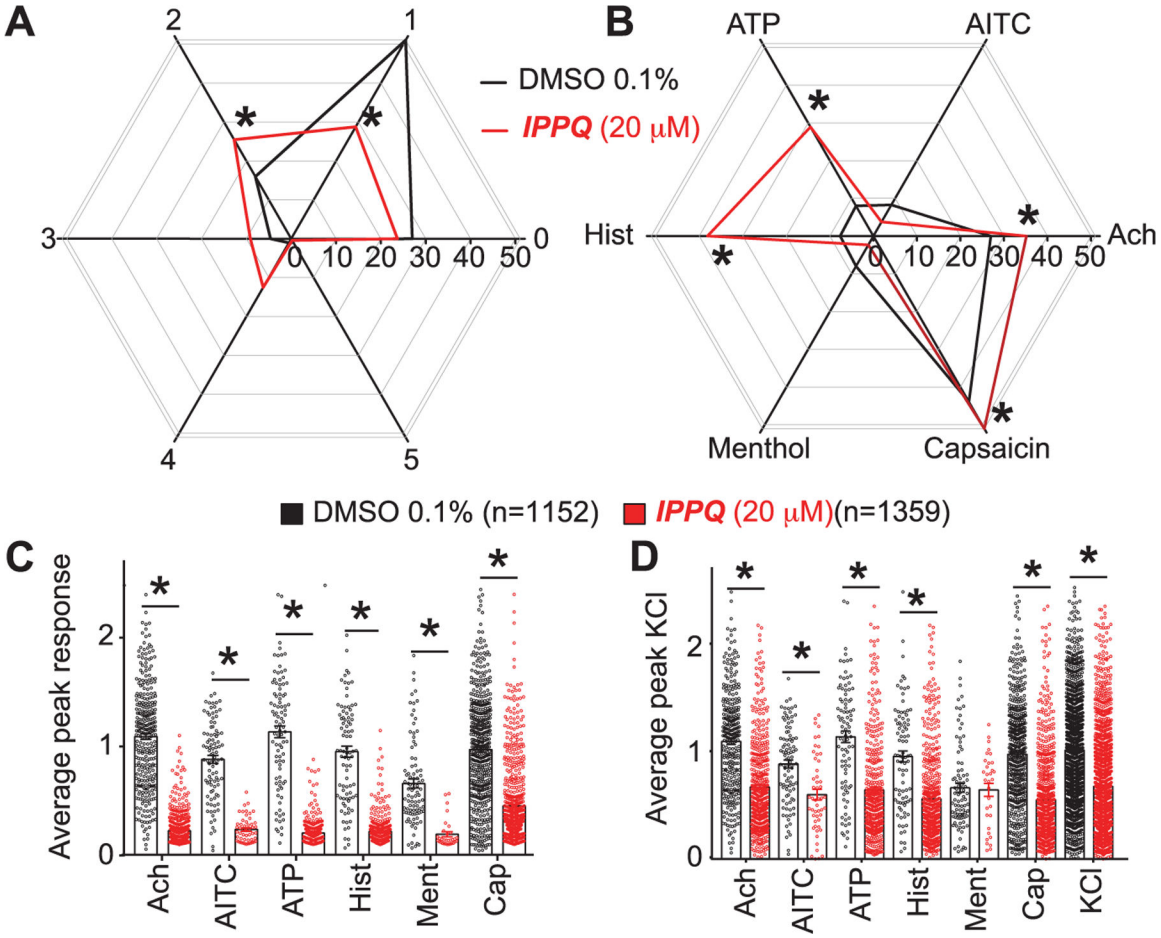

Figure 2.

Constellation pharmacology to identify potential off-target effects of *IPPQ*. Ca^{2+} imaging from DRGs treated overnight (15–18 hours) with 0.1% DMSO (n = 1152) or 20-μM compound *IPPQ* (n = 1359). These data include DRGs analyzed over 2 independent experiments with up to 9 trials per experiment. During each trial, >100 DRGs were sequentially stimulated for ~15 seconds (indicated by colored bars) with menthol (400 nM), histamine (50 μM), ATP (10 μM), allyl isothiocyanate (AITC) (200 μM), acetylcholine (1 mM), capsaicin (100 nM), and KCl (90 mM). Only DRGs responsive to membrane depolarization-evoked Ca^{2+} influx by KCl were included. Furthermore, only responses greater than 10% of baseline were included (indicated by filled black circles). (A) Analysis of DRG responses revealed the percentage of cells responding to the indicated number of molecular agonists, independent of which agonists elicited a response, in both DMSO- and *IPPQ*-treated conditions (n = 184–588, $*P < 0.001$, z-test.) (B) Analysis of DRG responses revealed the percentage of cells responding to the indicated molecular agonist, independent of any other agonist that also elicited a response, in both DMSO- and *IPPQ*-treated DRGs (n = 88–693, $*P < 0.01$, z-test). (C) Bar graph of average peak response to each of the indicated trigger. (D) Bar graph of the average peak response to KCl in DRG neurons responsive to the indicated trigger (n = 1152–1359, $*P < 0.05$, Student *t* test vs 0.1% DMSO). DRG, dorsal root ganglion.

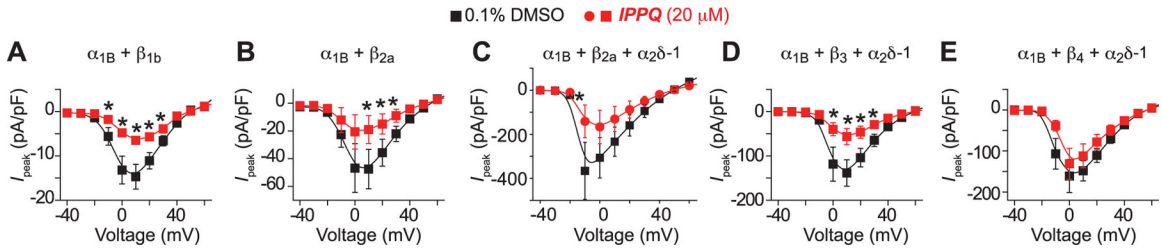

Figure 3.

IPPQ disrupts α1B–β1b, α1B–β2a, and α1B–β3–α2δ−1 interactions to inhibit Ca^{2+} currents. HEK293 cells expressing either (A) α1B + β1b, (B) α1B + β2a, (C) α1B + β2a + α2δ−1, (D) α1B + β3 + α2δ−1, or (E) α1B + β4 + α2δ−1 were subjected to an activation voltage step protocol to determine their I-V relationship after overnight (15–18 hours) treatment with 0.1% DMSO (black) or 20-μM *IPPQ* (red). Ca^{2+} currents in α1B + β1b, α1B + β2a, α1B + β2a + α2δ−1, and α1B + β3 + α2δ−1 expressing cells were significantly reduced in *IPPQ*-treated DRGs compared with 0.1% DMSO-treated counterparts (n = 5–18, $*P < 0.05$, Kruskal–Wallis test with Dunnett post hoc comparisons).

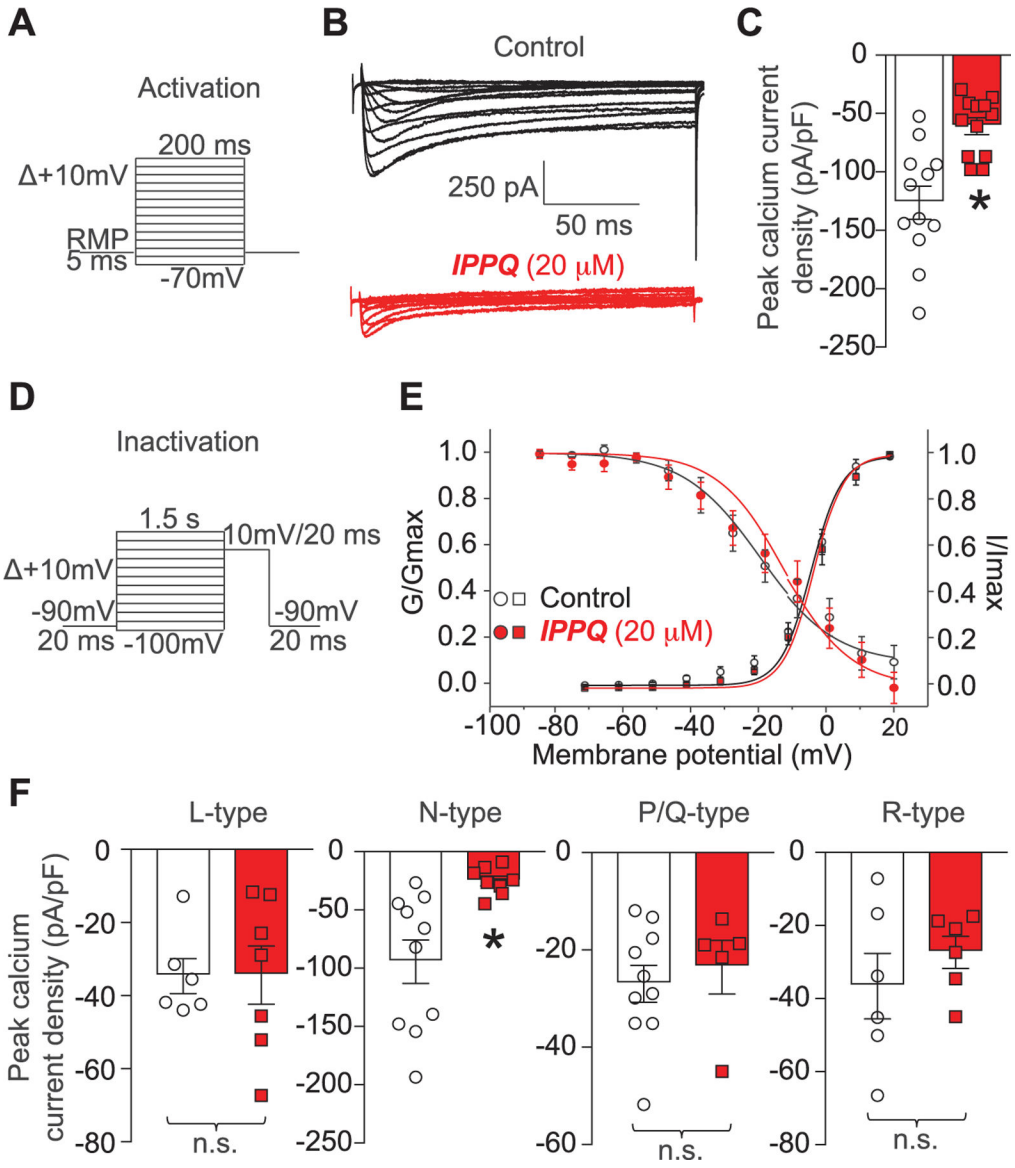

Figure 4.

IPPQ preferentially inhibits Ca^{2+} currents mediated by CaV2.2. (A) Activation (ie, current–voltage [I-V] relationship voltage step protocol). Cells were held at resting membrane potential for 5-ms before depolarization by 200-ms voltage steps from −70 to +60 mV in 10-mV increments. Currents were normalized to each cell's capacitance (pF). This allowed for collection of current density data to analyze activation of Ca^{2+} channels as a function of current vs voltage and peak current density. (B) Representative Ca^{2+} current traces from DRGs subjected to the activation protocol (shown in A). (C) Summary graph of peak Ca^{2+} current density (pA/pF) from DRGs incubated with 0.1% DMSO or 20-μM *IPPQ* overnight (15–18 hours) (n = 12; $*P < 0.05$, Kruskal–Wallis test with Dunnett post hoc comparisons). (D) Inactivation voltage-step protocol. Cells were held at −90 mV for 20 ms before depolarization by 1.5-second voltage steps from −100 to +10 mV in 10-mV increments, followed by a 20-ms pulse at 10 mV before returning to −90 mV for 20 ms.

(E) Normalized peak current plotted against its preceding holding potential and fitted with the Boltzmann relation. No significant differences were detected in half-maximal voltage or slope properties of either activation or inactivation between 0.1% DMSO and *IPPQ* conditions. (F) Summary graph of peak Ca^{2+} current density (pA/pF). Presence of *IPPQ* did not significantly reduce Ca^{2+} currents pharmacologically isolated through L-type, P/Q-type, or R-type Ca^{2+} channels. Presence of *IPPQ* significantly reduced N-type Ca^{2+} currents (compared with DMSO-treated DRGs, n = 6–10; $*P < 0.05$, Kruskal–Wallis test with Dunnett post hoc comparisons).

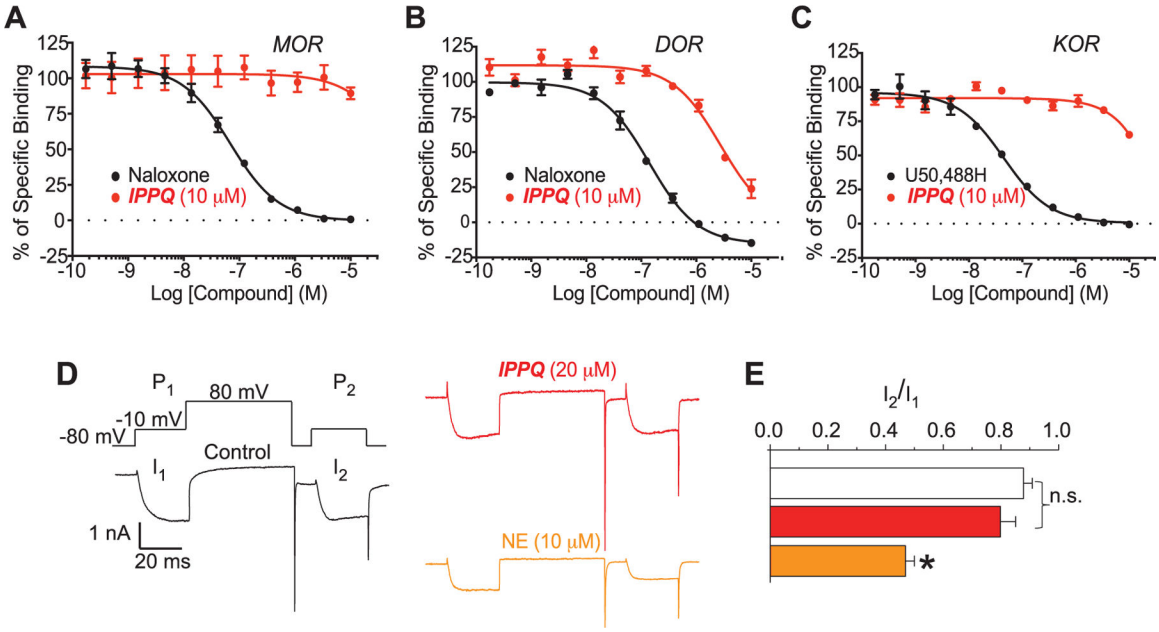

Figure 5.

IPPQ does not bind to opioid receptors and does not affect G protein–mediated inhibition of Ca^{2+} current in rat sensory neurons. Competition radioligand binding was performed in CHO cells expressing the human opioids receptors MOR (A), DOR (B), or KOR (C). Compound *IPPQ* or a positive control compound competed against ^{3}H-diprenorphine in all 3 cell lines. Curves reported as the mean ± SEM of the mean value from each individual experiment in N = 3 independent experiments. The K_I also reported as the mean ± SEM of the individual value from each of N = 3 independent experiments. (A) Compound *IPPQ* did not bind to the MOR. Naloxone K_I = 33.9 ± 1.7 nM. (B) Compound *IPPQ* produced 76.2% inhibition at 10 μM at the DOR, with an incomplete curve. This indicates an IC_{50} >3.3 μM and a K_I >1 μM. Naloxone K_I = 55.7 ± 6.7 nM. (C) Compound *IPPQ* did not appreciably bind to the KOR. U50488 K_I = 22.4 ± 4.1 nM. (D) Representative current traces following the “double pulse” protocol (*top*) for control, *IPPQ* (20 μM) applied for 30 minutes, and norepinephrine (NE, 10 μM). (E) Histograms of ratio of I_2/I_1, measured at 10 msec after the step to −10 mV of DRG neurons treated with 0.1% DMSO, *IPPQ*, or NE. *P, 0.05, Kruskal–Wallis test with Dunnett post hoc comparisons. DRG, dorsal root ganglion.

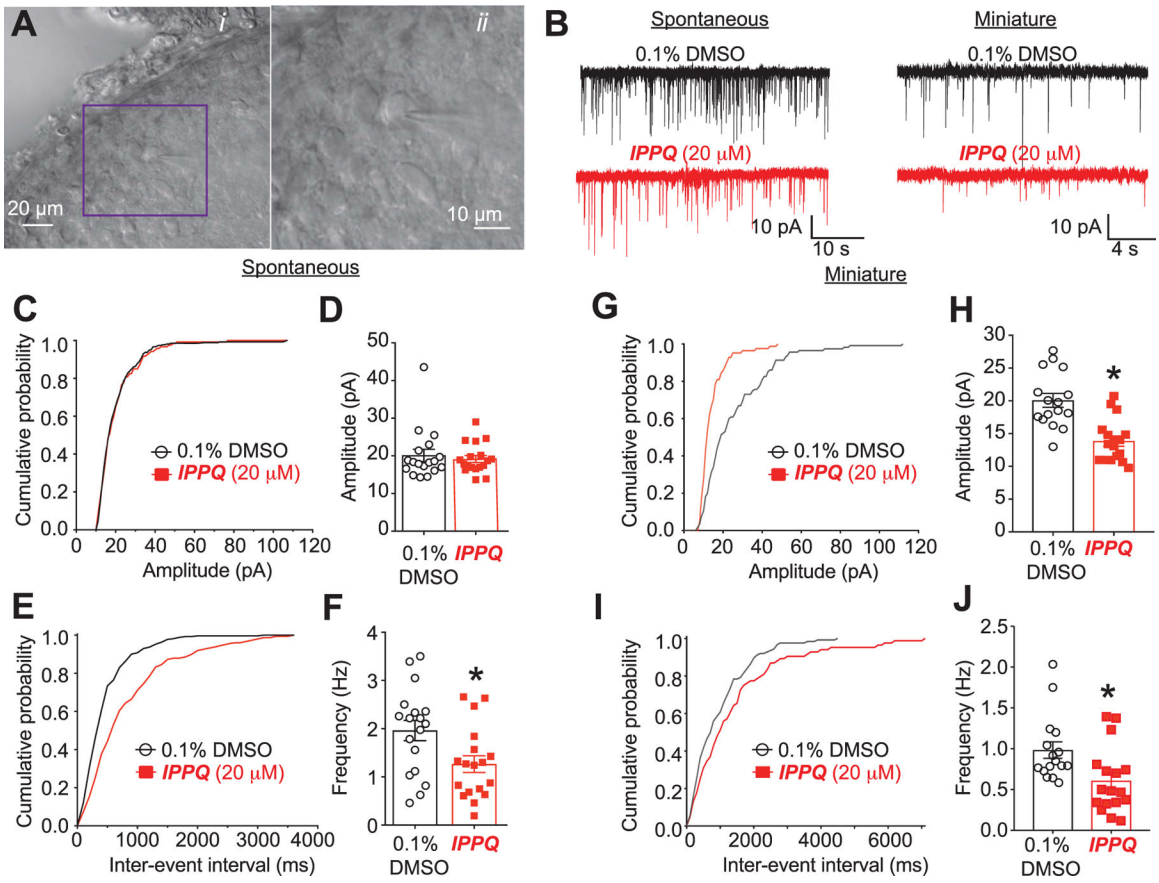

Figure 6.

IPPQ decreases spinal excitatory synaptic transmission. Photomicrograph of slice preparation showing that the *substantia gelatinosa* (SG) can be identified as a translucent pale band in the superficial dorsal horn enabling positioning of the recording electrode to this region. (A, i) infrared differential interference contrast image (IR-DIC) and (A, ii) image of the same cell (indicated by a purple red box in middle panel) with part of the recording electrode after whole-cell configuration. (B) Representative recording of spontaneous and miniature EPSCs traces of cells from the indicated groups: 0.1% DMSO or 20-μM *IPPQ*, applied through perfusion system during the experiment within 3 hours. The recordings were obtained within 30 minutes to 3 hours of drug perfusion; no difference was observed between recordings performed earlier vs later in the window after drug perfusion (data not shown). (C and D) The cumulative probability and summary of sEPSC amplitudes. (E and F) The cumulative probability of interevent interval and frequencies of sEPSCs for the indicated groups are shown. *IPPQ* treatment had no effect on the amplitude but decreased the frequency of the recorded sEPSCs. (G and H) The cumulative probability and summary of mEPSC amplitudes. (I and J) The cumulative probability of interevent interval and frequencies of mEPSCs. Both the frequency and amplitude of mEPSCs were decreased by 20-μM *IPPQ*. Data are expressed as mean ± SEM from n = 16 to 18 cells per condition. $^{*}P < 0.05$ (vs DMSO); Student *t* test.

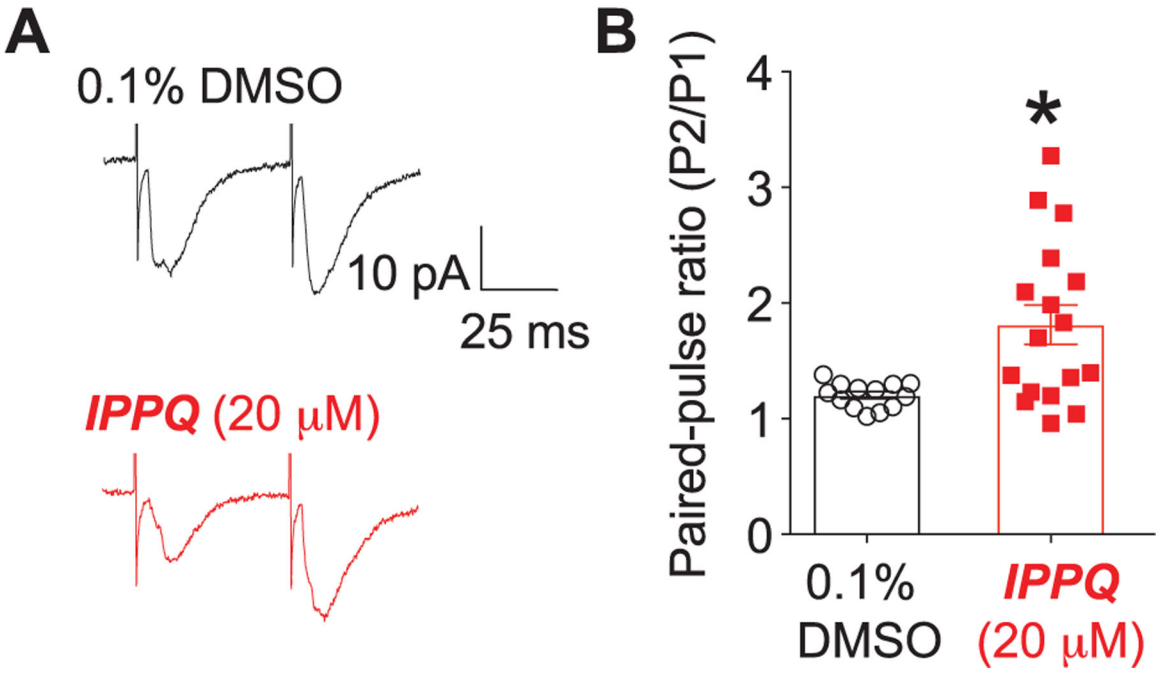

Figure 7.

IPPQ increases paired-pulse ratios. (A) Representative traces of paired-pulse ratio (PPR) from the indicated groups: 0.1% DMSO or 20-μM *IPPQ*. The recordings were obtained within 30 minutes to 3 hours of drug perfusion. (B) Summary of average PPRs from the indicated groups. Data are expressed as mean ± SEM from n = 13 to 17 cells per condition. **P* < 0.05 (vs DMSO); Student *t* test.

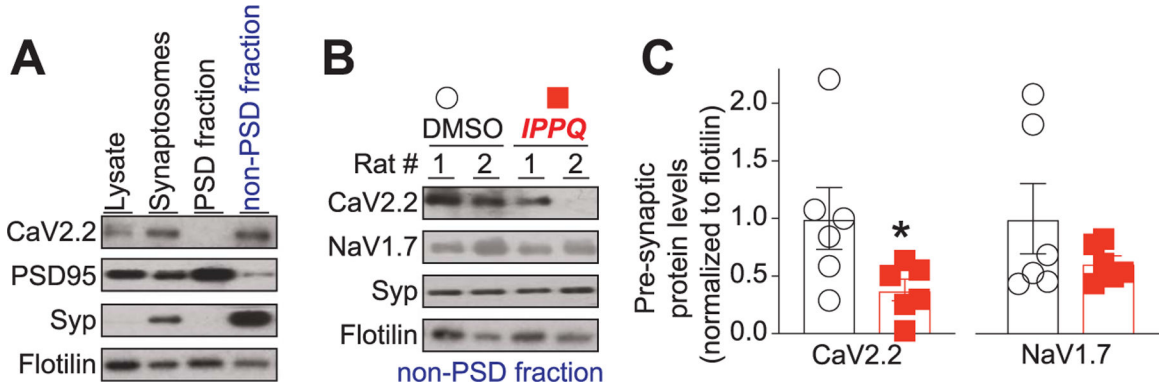

Figure 8.

IPPQ decreases CaV2.2 presynaptic localization in vivo and reduces evoked CGRP release from spinal cord. (A) Immunoblots showing the integrity of the synaptic fractionation from lumbar dorsal horn of the spinal cord. The non-postsynaptic density (non-PSD) fraction was enriched in the presynaptic marker synaptophysin (Syp), and the PSD fraction was enriched in the postsynaptic marker PSD95. The membrane-associated protein flotillin was used as a loading control. (B) Immunoblots showing the presynaptic CaV2.2 levels in the lumbar dorsal horn of the spinal cord of animals having received *IPPQ* (2 μg in 5 μL, intrathecally) compared with vehicle (0.1% DMSO). The synaptosomes were prepared from the dorsal horn of the spinal cord of rats 1 hour after injection with *IPPQ*. Synaptophysin shows the integrity of each fraction. Flotillin is used as a loading control. (C) Bar graph showing decreased CaV2.2 levels at the presynaptic sites of lumbar dorsal horn of the spinal cord in *IPPQ*-treated animals. Mean ± SEM, $*P < 0.05$, Mann–Whitney compared with the DMSO vehicle treatment.

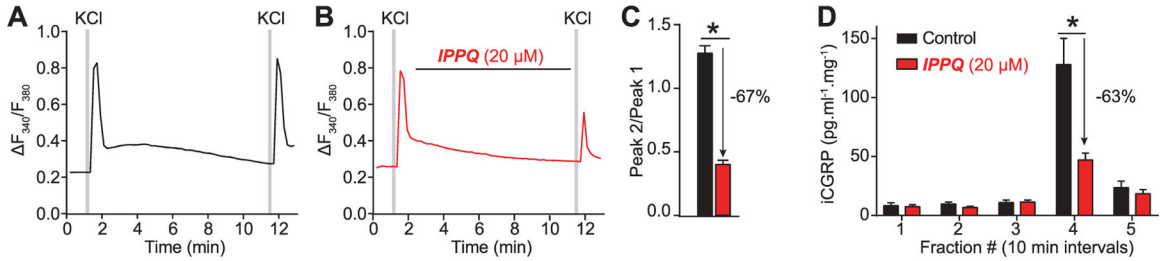

Figure 9.

IPPQ acutely reduces calcium influx and evoked calcitonin gene–related peptide (CGRP) release from spinal cord. (A) Representative traces of membrane depolarization-evoked Ca^{2+} influx by 90-mM KCl before and after 10 minutes application of either 0.1% DMSO (A) or 20-μM *IPPQ* (B). (C) Quantification of the peak ratio for the indicated condition. Ten-minute treatment with *IPPQ* significantly reduced the peak ratio (vs 0.1% DMSO, n = 460–493 cells, $*P < 0.05$, Student *t*-test). (D) CGRP released from spinal cord fractions collected every 10 minutes corresponded with the following conditions: 1-baseline, 2-baseline, 3-treatment, 4-treatment + 90-mM KCl, 5 wash. Previous treatment for 10 minutes with compound *IPPQ* significantly reduced high potassium-evoked CGRP release in spinal cord (vs DMSO, n = 4–5, $*P < 0.0001$, one-way ANOVA with Dunnett post hoc comparisons). ANOVA, analysis of variance.

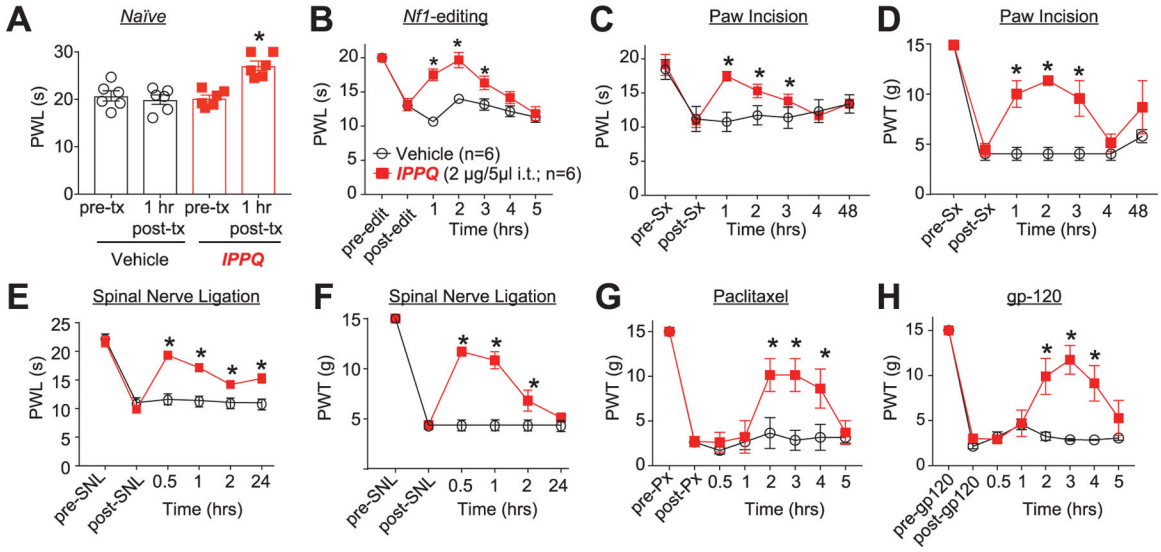

Figure 10.

IPPQ is antinociceptive in naive animals and reverses mechanical allodynia and thermal hyperalgesia in acute and neuropathic pain models. (A) Paw withdrawal latencies (PWLs) of naive rodents to a heat stimulus were significantly increased 1 hour after an intrathecal (i.t.) injection of *IPPQ* (2 µg) compared to animals injected with vehicle (10% DMSO, 10% Tween-80, 80% saline) (compared with i.t. injection of vehicle (n = 6, **P* < 0.05, 2-way ANOVA). (B) PWLs of rodents subjected to targeted Cas9-mediated editing of *Nf1* (using i.t. injection) were significantly decreased, but i.t. injections of *IPPQ* reversed this behavior (vs i.t. injection of vehicle, n = 6, **P* < 0.05, 2-way ANOVA). (C) PWLs of rodents that received a paw incision (Sx) on the left hind paw were significantly decreased. Intrathecal injection of *IPPQ* reversed this nociceptive behavior (compared with i.t. injection of vehicle, n = 6, **P* < 0.05, 2-way ANOVA). (D) Paw withdrawal thresholds (PWTs) of rodents that received a paw incision (Sx) on the left hind paw were significantly decreased. Intrathecal injection of *IPPQ* reversed this nociceptive behavior (compared with i.t. injection of vehicle, n = 6, **P* < 0.05, 2-way ANOVA). (E) PWLs of rodents that received a spinal nerve ligation (SNL) on the left hind paw were significantly decreased. Intrathecal injection of *IPPQ* reversed this nociceptive behavior (compared with i.t. injection of vehicle, n = 6, **P* < 0.05, 2-way ANOVA). (F) PWTs of SNL rodents were also significantly decreased. Intrathecal injection of *IPPQ* also reversed this behavior (vs i.t. injection of vehicle, n = 6, **P* < 0.05, 2-way ANOVA). (G) PWTs of rodents that received four 2-mg/kg intraperitoneal (i.p.) injections of paclitaxel (Px) over 12 days were significantly decreased. Intrathecal injection of *IPPQ* reversed this behavior (vs i.t. injection of vehicle, n = 6, **P* < 0.05, 2-way ANOVA). (H) PWTs of rodents were significantly decreased 15 days after receiving 3 i.t. injections of gp-120. Intrathecal injection of *IPPQ* reversed this behavior (vs i.t. injection of vehicle, n = 6, **P* < 0.05, 2-way ANOVA). The experiments were conducted in a blinded fashion. ANOVA, analysis of variance.

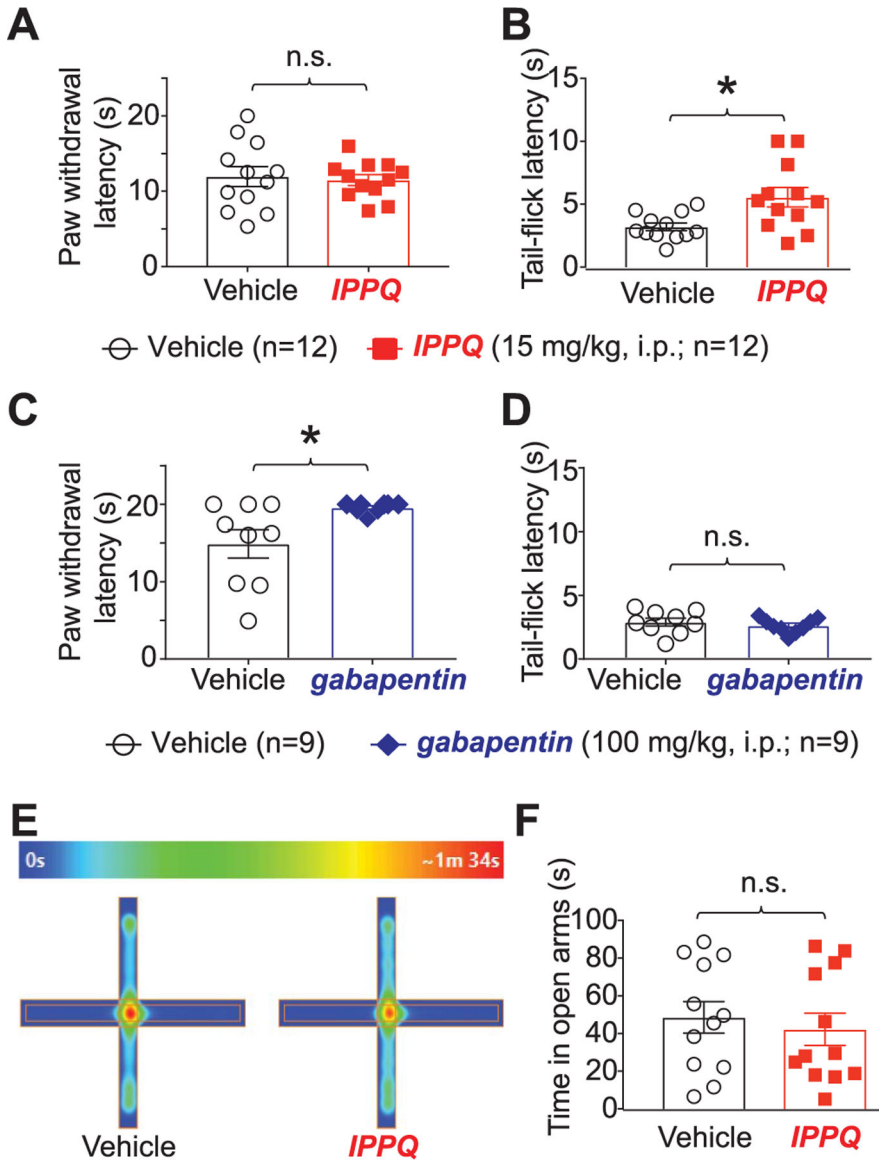

Figure 11.

IPPQ is analgesic in mice but does not affect anxiety-related behaviors. (A) Paw withdrawal latencies of naive mice in a hot-plate test (52°C) 75 minutes after injection of *IPPQ* (15 mg/kg) administered intraperitoneally (i.p.) were unaffected (compared with i.p. injection of vehicle: 10% DMSO, 10% Tween-80, 80% saline), n = 12, $P = 0.7583$, *t* test with the Welch correction. (B) Tail-flick latencies of naive mice to a hot (52°C) water bath 75 minutes after injection of *IPPQ* administered i.p. were significantly increased (vs vehicle i.p. injection), n = 12, $*P < 0.05$, *t* test with the Welch correction). (C) Paw withdrawal latencies of naive mice to the hot-plate test (52°C) 60 minutes after i.p. injection of gabapentin (100 mg/kg) administered were increased (compared with i.p. injection of vehicle), n = 9, $*P < 0.05$, Mann–Whitney test. (D) Tail-flick latencies of naive mice to a hot (52°C) water bath 60 minutes after i.p. injection of gabapentin (100 mg/kg) administered were unaffected (vs vehicle i.p. injection), n = 9, $P = 0.445$, *t* test with the Welch correction). (E) Naive mice

received an i.p. injection of *IPPQ* (15 mg/kg), or its vehicle and anxiety-related behaviors were assessed during 10 minutes in an elevated plus maze test. Heatmaps of the positions occupied in the elevated plus maze apparatus by treatment groups are represented in (E). (F) Bar graphs of the mean time spent in the open arms of the elevated plus maze. No differences were found between animals treated with *IPPQ* or with its vehicle ($P = 0.6014$, *t* test with the Welch correction, n = 12 mice/group). All experiments were conducted in a blinded fashion.